CONSTRAINING INFLATION THROUGH JOINT OBSERVATIONS OF THE PRIMORDIAL GRAVITATIONAL WAVE BACKGROUND

by

Jerod M. Caligiuri

B.S., Pennsylvania State University, 2003

M.S., University of Pittsburgh, 2013

Submitted to the Graduate Faculty of

the Kenneth P. Dietrich School of Arts and Sciences in partial fulfillment

of the requirements for the degree of

Doctor of Philosophy

University of Pittsburgh

2016

UNIVERSITY OF PITTSBURGH

DIETRICH SCHOOL OF ARTS AND SCIENCES

DEPARTMENT OF PHYSICS AND ASTRONOMY

This dissertation was presented

by

Jerod M. Caligiuri

It was defended on

Aug 3, 2016

and approved by

Arthur Kosowsky, Professor, Dept. of Physics and Astronomy, University of Pittsburgh

Andrew Zentner, Associate Professor, Dept. of Physics and Astronomy, University of Pittsburgh

Jefferey Newman, Associate Professor, Dept. of Physics and Astronomy, University of Pittsburgh

Adam Leibovich, Professor and Dept. Chair, Dept. of Physics and Astronomy, University of Pittsburgh

Tobias Marriage, Assistant Professor, Dept. of Physics and Astronomy, Johns Hopkins University

Dissertation Advisor: Arthur Kosowsky, Professor, Dept. of Physics and Astronomy, University of Pittsburgh

ABSTRACT

CONSTRAINING INFLATION THROUGH JOINT OBSERVATIONS OF THE PRIMORDIAL GRAVITATIONAL WAVE BACKGROUND

Jerod M. Caligiuri, PhD

University of Pittsburgh, 2016

The standard cosmological model leaves many questions unanswered. An early period of accelerated expansion of the Universe, referred to as inflation, resolves these issues. It provides a means to generate perturbations in matter and density that lead to the formation of structure as well as in gravitational waves. Inflation preserves fluctuations by driving them beyond the causal horizon. Their wavelengths trace the time they exit and their amplitude reveals the expansion rate and inflationary potential energy at exit. Measurements of these fluctuations is therefore a powerful probe of the inflationary Universe. After providing the necessary overview of background cosmology and inflation, I explore our ability to constrain viable models using joint measurements at vastly separated length scales and frequencies. Particular attention is paid to observations of the tensor power spectrum at large scales through measurements of the B-mode polarization of the cosmic microwave background and at small scales by direct detection using interferometric gravitational wave detectors. First, I consider a simple test of the inflationary consistency relation and discuss a simple means to constrain the running of the tensor spectral index. Secondly, I investigate more generally how joint observations can restrict viable models and reveal a highly constrained class of likely expansion histories and potential energies driving the expansion. Within these remaining classes of models, subsets are revealed by their spectral tilts at small scales. Thus, the addition of a measure of the tensor spectral tilt at solar system scales amplifies the restrictive power to identify valid inflationary models. I conclude with a discussion of the

possible addition of constraints of both the tensor and scalar power spectrum at intermediate scales and some for the challenges that future experiments will need to overcome.

TABLE OF CONTENTS

LIST OF TABLES

LIST OF FIGURES

Acknowledgments

I would like to take a moment to extend my deepest thanks to a lot people, without whom this work would never exist and my life would be unrecognizable.

My advisor, Arthur Kosowsky, and my committee members, Andrew Zenter, Jeff Newman, Adam Leibovich, and Toby Marriage, have been amazingly patient, supportive, and flexible. Thanks for tolerating my incessant questions no matter how ignorant they were.

My friends and colleagues Simone Aiola, Azarin Zarassi, Dritan Kodra, Kevin Wilk, Gen Sardane, Abhi Prakash, and Tim Licquia have made graduate school bearable. I am so glad that it brought us together and will always cherish the time that we shared. I hope our friendships endure no matter where our lives take us. To my friend Arthur Congdon, thank you for your encouragement to finish what I started and your selfless assistance throughout. Next, we will work on your book! Dave and Pam Ruediger, you have made my family's transition truly possible. Your love and selfless assistance have made these stressful times endurable. I consider you all not just friends, but family.

To my aunts and uncles, Rose, Al, and Lar Bisgoni, thank you for always helping and being there for me in your own ways. I would like to thank my grandmother Elizabeth Bisogni. You are one of the strongest women that I know. Your intensity and sharp wit will always be held close to my heart. My grandfather Mario (Eddy) Bisogni was and always will be an inspiration. I cannot begin to describe how much he meant to me. I would like to thank my sister, De'Anna. We have shared many struggles and have always been there to help each other persevere. I need to thank my mother, Marilyn. Words cannot describe how much you help me in all facets of life. I doubt it is possible for anyone to do more than you have done for me. My daughter, Ilaria, has inspired me never to stop reaching. You are a gift to the world. I hope that someday you reflect back on this accomplishment with

pride and a smile as I do when looking at you. My partner and love, Kristina, you have been the idealization of loving support. Graduate school was a difficult time for our family, but you never wavered in the face of all the challenges that it presented. I am so glad we are spending our lives together.

To you all, thank you so much. I wish you peace, love, and happiness.

This work is dedicated to my daughter, Ilaria.

Be curious.

Have fun!

PREFACE

All you really need to know for the moment is that the universe is a lot more complicated than you might think, even if you start from a position of thinking it's pretty damn complicated in the first place.

- Douglas Adams (1992). *Mostly Harmless*

We, as humans, have always struggled to understand the Universe and our place in it. The moment we believe we have figured something out, the more questions and complications arise. It is a constant spotlight on our ignorance but also an adventure with infinite avenues of revelation. Not long ago in the grandness of time, our view of the Universe was an earthen disk floating on a vast sea. Our perspective has grown to a potentially infinite Universe with potentially infinite worlds. This vastness is filled with ripples not unlike the sea of our human infancy. The cosmic postal service of particles, light, and gravity delivers to us postcards from foreign realms long ago, whose delivery times are restricted by a cosmic speed limit. Acceptance of these parcels gives a humble reminder of our ignorance while providing hints to help us on our journey toward enlightenment. Insight comes from all around us. We just need to know when and where to welcome it. Our ability to continue to find new ways to probe the unknown is a testament to human curiosity, tenacity, and ingenuity.

1.0 A BRIEF HISTORY OF STANDARD COSMOLOGY AND MOTIVATIONS

The standard cosmological model is a triumph of modern science, but there is still much to be learned. Today, evidence suggests that only about 5% of the content of the Universe is well understood. We can, however, confidently estimate the evolutionary history of the Universe all the way back to the first fractions of a second. Hubble's observational conclusion in 1929 that the Universe is expanding [7] and the accidental discovery of the residual light from an earlier hot, dense stage of the Universe by Penzias and Wilson in 1965 [8], and thereafter improvements of these measurements have continually generated support for this story.

Dark matter, first proposed by Zwicky in 1933 [9] (erroneously by Oort a year before [10]), was needed to explain the observed unexpectedly high velocites of galaxies in the Coma cluster. Later the presence of this unseen matter was suggested by the measurements of the rotation curve (velocity as a function of radius) of the Andromeda galaxy [11, 12]. Since then the presence of dark matter has found strong support in observations of gravitational lensing [13, 14], the cosmic microwave background (CMB hereafter) [15, 1], baryon acoustic oscillations [16], and the lyman-α forest [17]. The best estimates today suggest that roughly 85% of the matter content of the Universe is of this unknown form [1]. The quest to detect and constrain candidate models for dark matter has become an entire subfield of its own (see e.g. [18, 19, 20, 21] among many others).

Also puzzling is dark energy. First proposed as a cosmological constant by Einstein to ensure a static Universe [22], it was largely discarded after Hubble's confirmation of the Universe's expansion [7]. The more recent discovery of the acceleration of the expansion of the Universe by Perlmutter, Riess, Schmidt et.al. in 1998 [23, 24, 25] has brought about its rebirth in contemporary cosmology. In order to counteract the deceleration effects of

gravity due to the matter and radiation content of the Universe, the total energy content of the Universe must be dominated by something with a roughly constant energy density that effectively has a negative pressure. Best estimates today indicate that approximately 70% of the total energy content of the Universe is in this form [1].

The enigmas of dark matter and dark energy aside, the presence and overall quantity of them in the Universe is known with remarkable precision [1]. They have become pillars of the modern standard cosmological model, to the extent that it is referred to as Λ (dark energy) C (cold) D (dark) M (matter). Perhaps more puzzling than the nature of the majority of the Universe are the seemingly coincidental properties that our Universe has. What happened at the earliest moments of expansion and produce the Universe as it is today?

Despite the success of the standard cosmological model, new physics is needed to probe the natal moments of existence. This need is easily illustrated by the so-called monopole, horizon, and flatness problems; there is an abundance of literature on the subject so I will not go into great detail). The energy scales required to investigate the physical principles dominating this period of the Universe's evolution are beyond the reach of even the most optimistic of future earthly particle accelerator experiments. This leaves the detection of cosmological signatures as the best hope for gathering evidence to improve our understanding of this elusive piece of cosmic history. A leading theory to describe this early evolution is referred to as inflation.

Inflation is an accelerated period of expansion in the early Universe first proposed by Guth and others [26, 27, 28, 29, 30, 31, 32, 33, 34, 35]) in order to address the monopole, horizon, and flatness problems stated above. The past 25 years has seen a zoological kingdom of inflationary models proposed by theorists that typically involve one or more scalar fields driving the expansion.

This thesis is an investigation into the potential to probe the history of inflation using the relic gravitational wave background. Multiple observations at widely separated scales have the power to unveil the expansion history and the potential of the scalar field powering the expansion. I begin with an overview of the necessary background cosmology and present the basics of the cosmological problems that inflation solves in § 2. I continue with the fundamentals of scalar field inflation § 3. I include an overview of slow-roll approximations

as well as the generation of scalar and tensor perturbations that seed structure formation, anisotropies in the CMB, and the gravitational wave background. It is these tensor perturbations that provide a direct probe of the inflationary epoch free from the complications of baryonic physics ever present in studies of scalar perturbations. I then present two studies of how joint observations of tensor perturbations at vastly separated length (and frequency) scales can be used as a powerful probe of the nature and history of inflation in § 4, 5. I conclude in § 6 with a discussion of other prospects and future experiments that may move us closer to achieving the monumental goal of unveiling the earliest moments of time.

2.0 THE BASICS OF STANDARD COSMOLOGY AND ITS PROBLEMS

2.1 INTRODUCTION

Standard cosmology tells the tale of the Universe's history back to a time when it was $\sim 10^{-12}$ seconds old. This model is built upon the assumption that the Universe is homogeneous and isotropic. Based on these assumptions, we can write a metric that is invariant under rotation and translation. Maintaining a static comoving spatial geometry, the evolution of the spacial Universe is contained within the scale factor, $a(t)$. This is the Friedmann-Lemaître-Robertson-Walker (FLRW) metric, and can be written

$$\begin{aligned} ds^2 &= dt^2 - a(t)^2 dx^2 && (2.1) \\ &= dt^2 - a(t)^2 \left[\frac{dr^2}{1-kr^2} + r^2 d\Omega^2 \right] && (2.2) \end{aligned}$$

in Cartesian and spherical coordinates respectively. Here k describes the curvature of the Universe. For $k = -1, +1$, or 0 the Universe is open, closed, or flat. The variables x and r represent comoving distance in Cartesian and spherical coordinates, and $d\Omega = \sin\theta d\theta d\phi$ is the solid angle on the sphere. I have chosen the unit convention of setting $c = k_B = \hbar = 1$ and will continue to do so throughout unless otherwise noted.

From General Relativity we have Einstein's field equations:

$$G_{\mu\nu} = 8\pi G T_{\mu\nu}. \tag{2.3}$$

Here $G_{\mu\nu}$ is called the Einstein tensor, G is Newton's gravitational constant, and $T_{\mu\nu}$ is the stress-energy tensor. In an FLRW spacetime,

$$T^{\mu}{}_{\nu} = \begin{pmatrix} \rho & & & \\ & -p & & \\ & & -p & \\ & & & -p \end{pmatrix}, \tag{2.4}$$

where ρ is energy density and p is pressure. Remember that we are working with $c = 1$ and so these are of the same units. Conserving stress-energy by taking its covariant derivative we find the continuity equation:

$$\dot{\rho} + 3(\rho + p)\frac{\dot{a}}{a} = 0. \tag{2.5}$$

It is standard to define an equation of state such that

$$p = w\rho. \tag{2.6}$$

For pressureless matter $w = 0$, for radiation $w = 1/3$, and for a negative pressure cosmological constant $w = -1$. The continuity equation together with Einstein's field equations provide:

$$\left(\frac{\dot{a}}{a}\right)^2 = \frac{8\pi}{3m_{pl}^2}\rho - \frac{k}{a^2} \tag{2.7}$$

$$\frac{\ddot{a}}{a} = -\frac{4\pi}{3m_{pl}^2}(\rho + 3p). \tag{2.8}$$

These are referred to as the Freidmann and Raychaudhuri equations, respectively. If we consider the Raychaudhuri equation, which describes the acceleration of the Universe, and only consider cases of matter, radiation, and Λ domination, we find that for matter and radiation, $\ddot{a} < 0$. The expansion is slowing down. For the case with only dark energy, $\ddot{a} > 0$. The expansion rate is increasing. In general, the energy density in Eqs. (2.4), (2.5), and (2.8) represents the total energy density of the Universe. This is the sum of matter, radiation, and dark energy. Knowing that matter scales as a^{-3}, radiation as a^{-4}, and dark energy remains constant, we can replace ρ with this sum and their scaling relation. It is standard to define the Hubble parameter $H \equiv \frac{\dot{a}}{a}$. We can also define the critical density to be that where $k = 0$,

$\rho_{crit} \equiv \frac{3m_{pl}^2 H^2}{8\pi}$ such that a Universe at this density will expand asymptotically to a halt. If we scale the energy densities to the critical density, we can then define $\Omega \equiv \frac{\rho}{\rho_{crit}}$. We can also define $\Omega_k \equiv -\frac{k}{(aH)^2}$. Given these definitions, scaling to the critical density today, setting the scale factor today to $a_0 = 1$, and calling the Hubble parameter today H_0, we arrive at a convenient form of the Freidmann Equation:

$$H^2 = H_0^2 \left(\Omega_M a(t)^{-3} + \Omega_R a(t)^{-4} + \Omega_\Lambda + \Omega_k a(t)^{-2}\right), \tag{2.9}$$

where $\Omega_{M,R,\Lambda,k}$ are the energy densities of matter, radiation, dark energy, and curvature respectively today scaled to today's critical density. Note that the energy density due to matter includes both baryonic matter and dark matter ($\Omega_M = \Omega_b + \Omega_{DM}$). From the above definitions and the Freidmann equation in Eq. (2.8), it can also be show that $\Omega_k = 1 - \Omega$ at any time, where $\Omega = \Omega_M a(t)^{-3} + \Omega_R a(t)^{-4} + \Omega_\Lambda$. The Planck collaborationhas provided the strongest current constraints on these parameters [1]. These are presented in Table (1).

Table 1: Cosmological parameter constraints from Ref. [1]. Errors are presented at 68% confidence unless otherwise indicated. the Hubble parameter describing the expansion rate of the Universe is given by H_0. Ω's are energy densities scaled to the critical density in the Universe today. Ω_b, DM are the scaled energy densities of baryonic and dark matter, respectively, such that $\Omega_b + \Omega_D M = \Omega_M$. $\Omega_{\Lambda,R,k}$ are the relative energy densities of dark energy, radiation, and curvature.

$H_0(\text{kms}^{-1}\text{Mpc}^{-1})$	67.74 ± 0.46
Ω_b	0.048598 ± 0.000305
Ω_{DM}	0.258896 ± 0.002179
Ω_Λ	0.6911 ± 0.0062
Ω_R	$9.17 \pm 1.9 \times 10^{-6}$
Ω_k	0.0008 ± 0.0013

General relativity, the metric, and the Freidmann equation create the foundation that modern cosmology is built upon. The above described enables us to unlock the history of our Universe *almost* entirely. Those still unrevealed moments are the focus of this work.

2.2 HORIZONS AND TIME

Using the Freidmann equation, it is a simple task to solve for $a(t)$. When considering this with the metric, we can determine the comoving distance a photon would travel in some amount of time since the Big Bang. As this is the absolute farthest any information or particle can travel in the indicated amount of time it is known as the (comoving) cosmological horizon, determined by

$$d_H(t) = \int_0^t \frac{dt'}{a(t')}. \tag{2.10}$$

The proper (physical) horizon size is simply the comoving horizon times the scale factor.

We can look at the simple examples of the Universe being dominated by only one type of energy. When dominated by matter, $d_H \propto t^{1/3}$, when dominated by radiation $d_H \propto t^{1/2}$, and a Universe with only dark energy will have $d_H \propto e^{-H_0 t}$. For the cases of matter or radiation domination, the comoving horizon grows. However for a Universe having only a cosmological constant, the comoving horizon actually shrinks. Because the Universe has recently become dominated by dark energy, the horizon is now shrinking. What this implies is that as the horizon grows, more space is inside of it and therefore causally connected to everything else within the horizon. Now that our comoving horizon is shrinking, regions of space are being driven out of contact from our region of the Universe (the Hubble volume).

Not only can we describe the size of the causally connected region of the Universe at any time, but we can also describe its age. We can solve for proper time and age if we scale the solution to the Freidmann equation such that $a_0 = 1$. It is often convenient to introduce a temporal analog to comoving distance, called conformal time:

$$d\tau = \frac{dt}{a(t)}. \tag{2.11}$$

Note that in units with $c = 1$, the conformal time τ defined by Eq. 2.11 is equal to the comoving horizon, Eq. 2.10.

2.3 PROBLEMS IN STANDARD FLRW COSMOLOGY

Despite the power and successes of the standard cosmological paradigm, there are issues that still exist. Why are massive monopoles not observed? Why is the Universe so flat? Why is the Universe so smooth when at recombination patches across the sky were out of causal contact? How are the slight perturbations that lead to structure formation generated? Without answers to these questions, we are left with a set of specific, possibly coincidental, initial conditions that some would try to explain through the anthropic principle. I do not find this answer to be acceptably scientific. In this section I provide a brief overview of these issues but save their resolution by inflation for § 3.

2.3.1 The Monopole Problem

A general gauge theory theorem states that the breaking of any group to the standard model gauge group will result in nonperturbative, stable field configurations called monopoles; these are point-like topological defects with an effective mass of (e.g. $m \sim 10^{16}$ GeV) determined by the symmetry breaking scale (temperature of $T \sim 10^{14}$ GeV). This massive monopole is surrounded by a magnetic field with non-zero divergence (an effective magnetic charge) [36]. The Kibble mechanism [37] implies that a lower bound on their spatial density should be around one per horizon volume at the time of symmetry breaking. This will lead to the dominance of matter in the energy content of the Universe that is well above the critical density, causing a halt of expansion and a recollapse. This is clearly not the case. The absence of monopoles requires a particular initial configuration or a mechanism to dilute their presence into negligibility.

2.3.2 The Flatness Problem

Observations reveal that the Universe has a conveniently simple Euclidean spacial geometry. It is flat [1]. When the Universe is dominated by an energy density that results in a negative pressure, the geometry is driven further toward flattness. Despite the fact that we are currently in an epoch that is dominated by such an energy density (dark energy), this has

not been the case for the majority of cosmic history. During periods where the Universe is dominated by matter or radiation, curvature grows. The evolution of curvature with respect to the scale factor is given by

$$\frac{d|\Omega_k|}{d\ln a} = (1+3w)|\Omega_k|(\Omega_k+1), \tag{2.12}$$

where Ω_k and a are the unitless curvature density and scale factor respectively. The equation of state parameter is given by $w = 0, 1/3, -1$ for matter, radiation, and dark energy. This is discuss further in § 3.1.3. Notice that if $w > -1/3$ curvature grows. In order to arrive at a flat Universe after an extended period of evolution governed by matter or radiation, these periods must have begun in a state of flatness. Considering the fact that curvature has been increasing over the majority of cosmic evolution, the curvature when the Universe was 10^{-12} seconds old would have to have beeen $\Omega_k \lesssim 10^{-60}$ [36]. Flatness is a unstable condition unless expansion is accelerating. If the Universe were in fact not flat at the onset of radiation and matter domination, it would either recollapse on itself or be driven apart before structures could form as they exist today. Can we generalize the geometry of the Universe and still end in flatness or was this simply a particular initial condition?

2.3.3 The Horizon Problem

The CMB is the residual light released when photons decoupled and fell out of equilibrium with matter ($z_{dec} \approx 1100$ or $a(t_{dec}) \sim 10^{-3}$). Of course since then the light has redshifted by the same factor of $\sim 10^3$ in wavelength. The slight density fluctuations in matter that eventually lead to structure formation correspond directly to temperature fluctuations in the CMB sky if the perturbations are adiabatic. The observed temperature of the CMB today is $T_{CMB} = 2.725 \pm 0.002$ K [2] with fluctuations first measured by the COBE mission to be $\Delta T/T \sim 10^{-5}$ [38]. Directions separated by more than 1° on the sky today trace back to points at last scattering which have separations larger than the horizon at that time. Those points cannot have ever been in causal contact during the expansion history of the standard cosmological model.

2.4 OBSERVED PERTURBATIONS

As discussed in the previous section (§ 2.3.3), the Universe (and CMB) is extremely uniform and smooth. There are, however, fluctuations. These fluctuations are $\sim 10^{-5}$. It is common practice to represent these at any point on the sky as a spherical harmonic expansion:

$$\frac{\Delta T(\hat{n})}{T} \equiv \Theta(\hat{n}) = \sum_{l=2}^{\infty} \sum_{m=-l}^{l} a_{lm} Y_{lm}(\hat{n}), \tag{2.13}$$

Where $\Delta T(\hat{n})$ is the temperature fluctuation about the mean CMB temperature, T, in the location $\hat{n}$ on the sky. The summation begins at $l = 2$ because the monopole represents the average all sky CMB temperature and the dipole is due to the doppler shifting as a result of the motion of our solar system. This representation of the temperature perturbations is a unitless quantity, but it is also typical to multiply Eq. (2.13) by the temperature of the CMB in units of μK. To very good approximation, these anisotropies appear to be consistant with a Gaussian random field [39].

The Planck experiment observed the CMB at a remarkable $\approx 3'$ scale resolution which is shown in Fig. 1 [3]. The mean CMB temperature and the dipole due to the motion of the solar system have been subtracted. The non-blackbody spectrum of the galactic emission has enabled its removal, and a best-fit blackbody projection is present in its stead. The hot and cold spots are the relative fluctuations to the average CMB temperature ($\approx 2.725 \pm 0.002$K [2]).

We can statistically characterize the CMB sky using only the angular power spectrum:

$$\delta_{ll'}\delta_{mm'}C_l \equiv \langle a_{lm} a^*_{l'm'} \rangle \,. \tag{2.14}$$

The average in 2.14 is over an imagined ensemble of CMB skies in a statistically homogeneous Universe. We only have 1 observable sky, so we can estimate the power spectrum by averaging over the $2l + 1$ values of m:

$$C_l = \frac{1}{2l+1} \sum_m |a_{lm}|^2. \tag{2.15}$$

.

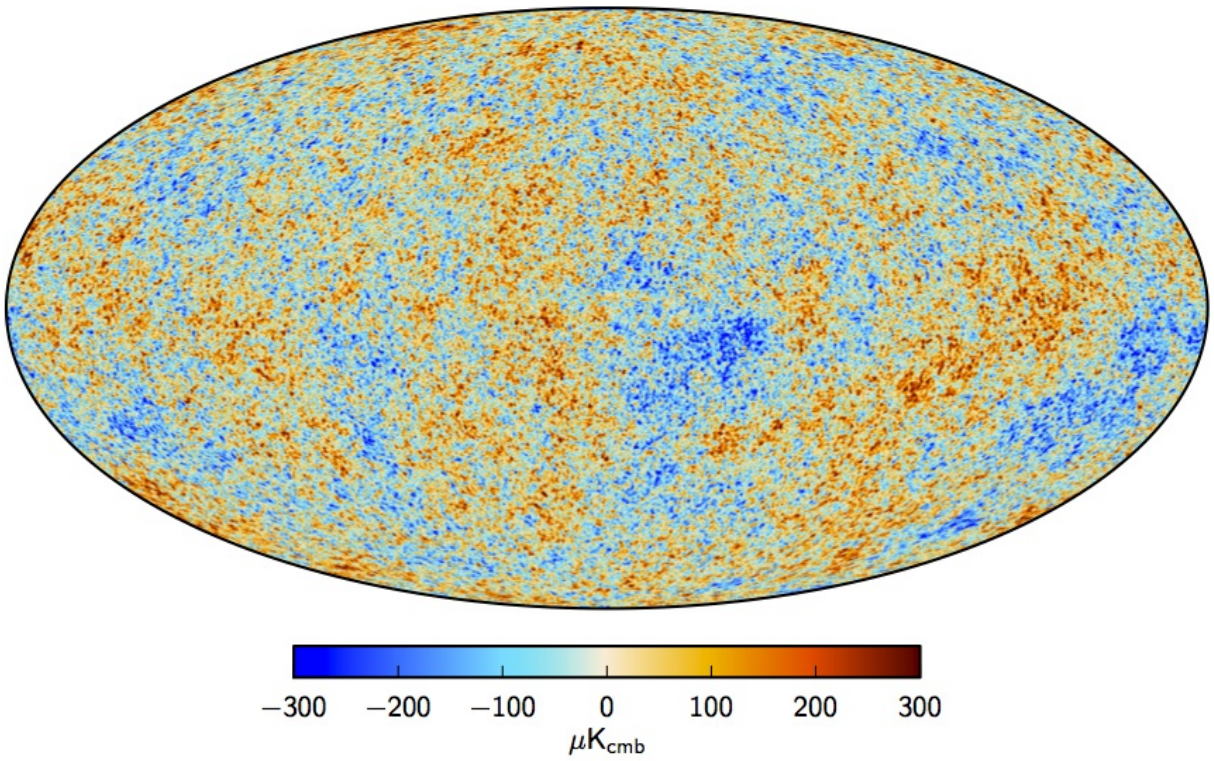

Figure 1: The CMB sky (temperature) as seen by the Planck experiment [3]. The mean temperature and dipole due to motion have been removed. The galactic signal has been removed and replaced with a best-fit blackbody signal that maintains the same statistics of the rest of the CMB sky. Image courtesy of ESA and the Planck Collaboration.

The temperature spectrum peaks at $l \approx 200$ corresponding to the fluctuations on degree scale patched in the CMB sky, which is the horizon size at the time of decoupling. If these are modes that have just entered the horizon at that time, they have not had time to thermalize with their surroundings or dilute with expansion prior to last scattering. Correlations at larger angular scales are also present. These are the effects of modes entering the horizon after decoupling. These large angle correlations are directly linked to the horizon problem described in § 2.3.3.

We observe anisotropies as a 2D spherical slice of 3D primordial perturbations. Density perturbations cause localized gravitational wells. Photons exiting these regions at last scat-

tering are thus redshifted and result in the observed CMB temperature fluctuations. These 3D fluctuations can be represented as the power spectrum $P(\vec{k})$. The power spectrum is defined by

$$\left\langle X(\vec{k})X^*(\vec{k'})\right\rangle = \frac{2\pi^2}{k^3}P_X(\vec{k})(2\pi)^3\delta^3(\vec{k}-\vec{k'}), \tag{2.16}$$

where $X(\vec{k})$ is some dimensionless field, for example curvature perturbation (which is related to the fractional density perturbation on scales inside the horizon) or tensor perturbation amplitudes, and $\vec{k}$ are the continuous Fourier mode vectors. In an isotropic Universe, $P(\vec{k}) \rightarrow P(k)$ because of the absence of directional dependence. Observations of C_l's thus put constraints on $P(k)$, the primordial power spectrum of perturbations (e.g. see [40]). I will focus on $P(k)$ rather than C_l but address them here to reinforce the fact that the C_l's are the directly observed quantities. The characteristic parameters of $P(k)$ (to be discussed later) are constrained from these observation.

If the fluctuations are adiabatic, the clumps of dark matter, baryonic matter, and radiation will all coincide on the same locations with the same fractional densities resulting in a net curvature perturbation. Isocurvature (also referred to as entropy) perturbations, on the other hand, do not require coincident perturbations of the same fractional densities. Such a case will not result in curvature perturbations but rather the same total curvature everywhere. Adiabatic perturbation peaks in the temperature and polarization power spectra are anticorrelated which would not be generically true for entropy perturbations [41]. Current observations are consistent with perturbations being adiabatic [40].

Anisotropies are not only present in the temperature of the CMB but also in polarization. This is the result of Thomson scattering of unpolarized photons incident from multiple directions simultaneously. If the intensity were equal, the resulting light would be fully unpolarized. However, due to the presence of anisotropies with a quadrapole component during last scattering, there are slight differences in the incident light intensity, resulting in a net polarization after Thomson scattering.

Polarization of the CMB is broken into two components: a gradient mode (E-mode) and a curl mode (B-mode) [42, 43]. Such orientations are 45° rotations from each other. These modes are orthogonal combinations of the Q and U Stokes parameters for linear polarization

(also 45° rotations from each other). We can expand combinations of these in terms of spin weighted spherical harmonics as

$$Q(\hat{n}) \pm iU(\hat{n}) = \sum_{l=2}^{\infty} \sum_{m=-l}^{l} a_{lm}^{\pm} Y_{lm}^{\pm}(\hat{n}). \tag{2.17}$$

We can therefore define the E and B polarization modes in terms of these expansion coefficients:

$$a_{lm}^{\pm} = a_{lm}^{E} \pm i a_{lm}^{B}. \tag{2.18}$$

As with temperature perturbations, this spherical expansion of polarization enables the characterization of E and B-modes with angular power spectra as defined in Eq. (2.14). The temperature and polarization auto and cross power spectra are shown in Table 2.

Table 2: The temperature and E and B mode polariation angular power spectra.

Auto Spectra	Cross Spectra
$\delta_{ll'}\delta_{mm'}C_l^{TT} \equiv \langle a_{lm}^{T} a_{l'm'}^{T*} \rangle$	$\delta_{ll'}\delta_{mm'}C_l^{TE} \equiv \langle a_{lm}^{T} a_{l'm'}^{E*} \rangle$
$\delta_{ll'}\delta_{mm'}C_l^{EE} \equiv \langle a_{lm}^{E} a_{l'm'}^{E*} \rangle$	$\delta_{ll'}\delta_{mm'}C_l^{TB} \equiv \langle a_{lm}^{T} a_{l'm'}^{B*} \rangle$
$\delta_{ll'}\delta_{mm'}C_l^{BB} \equiv \langle a_{lm}^{B} a_{l'm'}^{B*} \rangle$	$\delta_{ll'}\delta_{mm'}C_l^{EB} \equiv \langle a_{lm}^{E} a_{l'm'}^{B*} \rangle$

There are two conventions typically used to describe these CMB polarization modes. Here I have chosen to employ spin 2 spherical harmonics due to the relative polarization orientations of the Q and U Stokes parameters and their transformation properties under rotations [44]. The other convention is to write these quantities in terms of the polarization tensor, thus requiring the use of tensor spherical harmonics [45]. The expansion (regardless of the convention of choice) enables us to formulate power spectra for polarization analogously to temperature. The computation of the expansion coefficients can be done using readily available public codes such as CMBFast [5], CAMB [4, 46] and CLASS [6]. To visualize these polarization modes, I have simulated a low resolution CMB sky using CAMB [4, 46] and

overlaid the polarization vectors. Fig. 2a only contains E-mode polarization while Fig. 2b has polarization vectors rotated by 45° to convert the E-modes in Fig. 2a into pure B-modes.

The primordial E-modes are primarily sourced by the same density (or scalar) perturbations with only a small contribution from tensor just as the temperature anisotropies. The primordial B-modes, however, are most commonly considered to be sourced by tensor perturbations, peaking at a multipole of $l \approx 80$. Identifying the primordial power spectrum (tensor or scalar) requires precise characterization of the foreground contributions to the observed signals. This is particularly difficult with B-modes, as the foreground signals dominate observations. B-mode producing galactic dust and the conversion of E-modes to B-modes by gravitational lensing of CMB photons by large scale structure dominate the signal at all scales. The lensing signal peaks at $l \approx 1000$. Both of these signals have been detected in B-mode polarization (e.g. [51, 148]). Lensing has also been measured by exploiting its non-Gaussian nature (e.g. [142]) and through its correlation with large scale structure (e.g. [141]).

Figure 3 (courtesy Lyman Page) shows the most up to date, as I write this, compilation of power spectra data from the Planck, ACTPol, SPTPol, BICEP2/Keck, and Polarbear experiments. The increase in error at small multipoles (large angular scales) is unavoidable. This is referred to as cosmic variance and is the result of low sampling. After all, we only have one sky. This limits the information that can be obtained on the largest of scales, and no amount of technological advancement will be able to overcome it.

Troublesome as of late is the presence of B-mode producing dust. Efforts are underway to characterize the dust in order to find the possible signal that lies beneath (for example, see [51]). To date primordial B-mode polarization of the CMB has not been positively detected.

If it were not for the presence of perturbation in the Universe, you would not be reading this. Gravitational attractions would never have been strong enough to cause regions to collapse and structures to form. ΛCDM gives no explanation of the existence of these anisotropies. This too leads to the initial condition question. Again, we need to go beyond standard cosmology in an attempt to explain the observed anisotropies and consequently the structures that exist in the Universe.

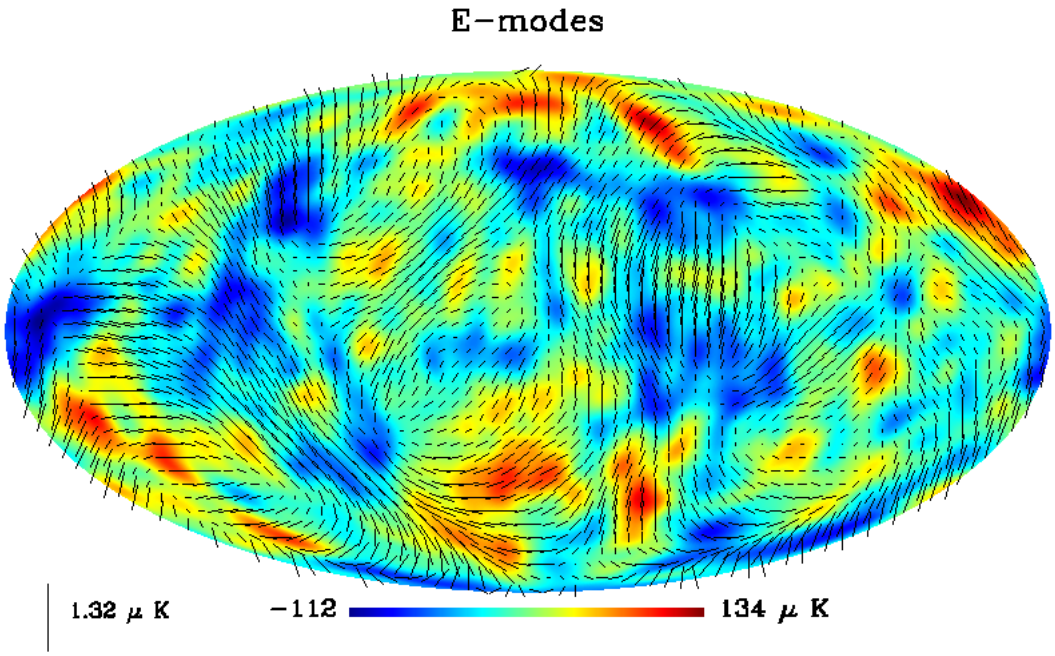

(a) CMB sky with only E-mode polarization.

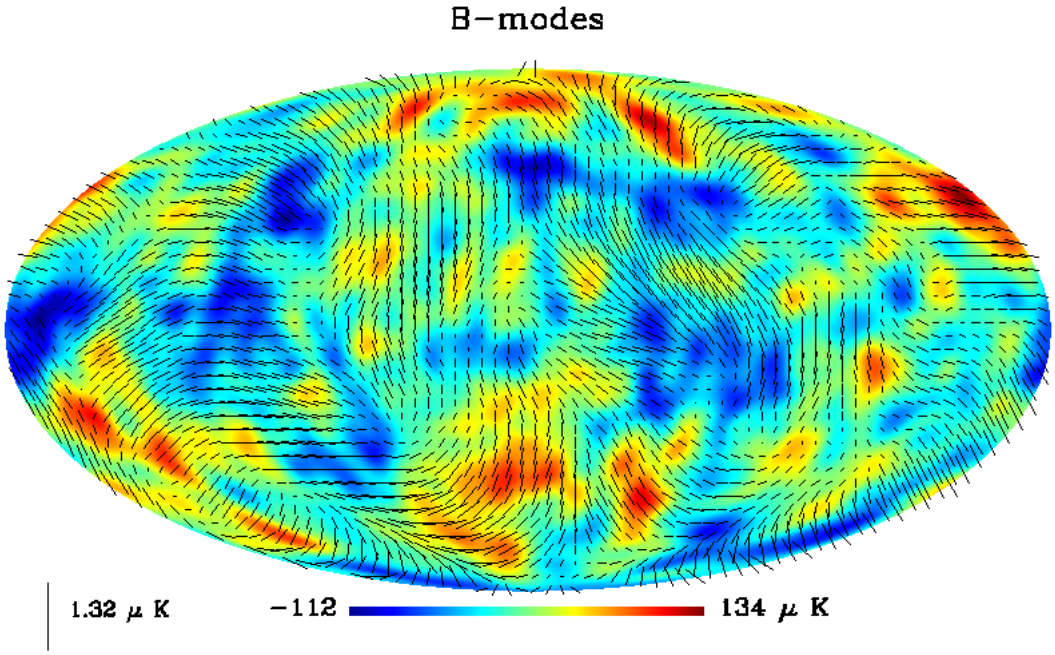

(b) CMB sky with on B-mode polarization.

Figure 2: Simulated CMB sky using CAMB [4]. Polarization vectors are plotted over the temperature map.

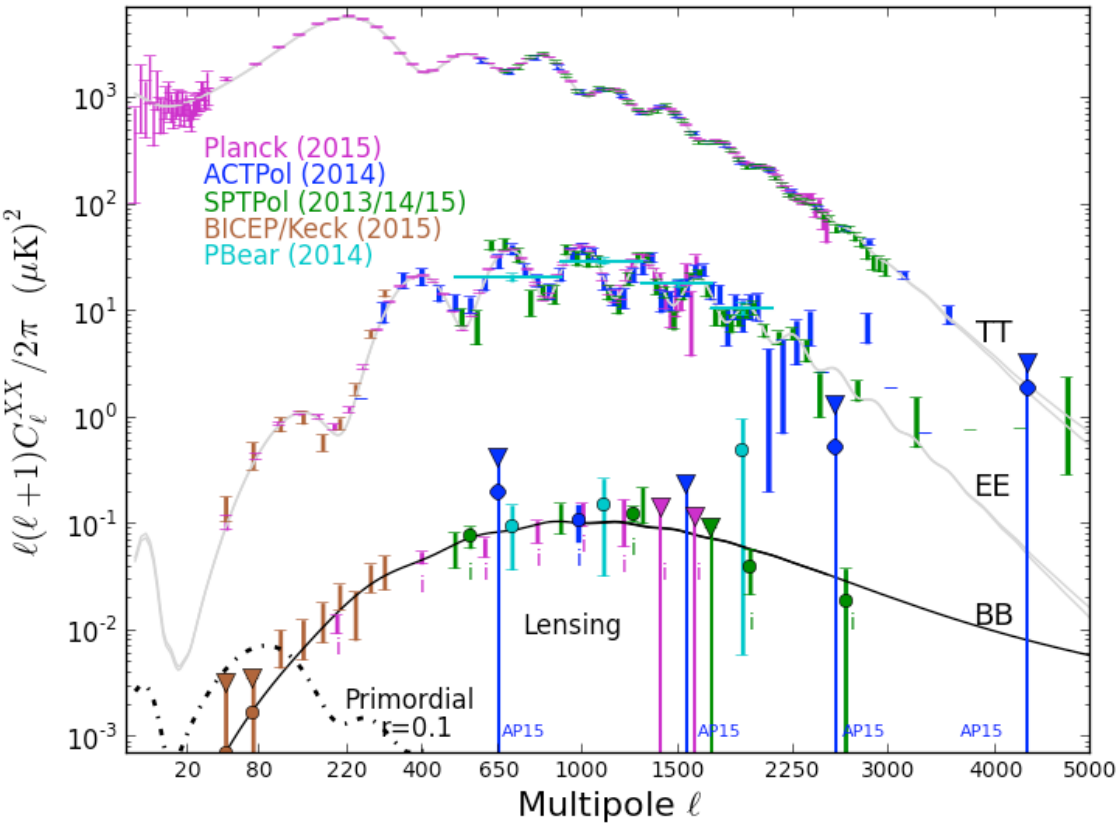

Figure 3: The most recent compilation of CMB power spectra data from Planck, ACTPol, SPTPol, BICEP2/Keck, and Polarbear. This includes TT, EE, and BB power spectra (courtesy Lyman Page).

3.0 INFLATION

Inflation is a period of accelerated expansion in the early Universe. For inflation to be a viable solution it needs to have specific characteristics. It needs to resolve the monopole, flatness, and smoothness issues as well as provide a means to generate the perturbations that seed structure formation. Another crucial requirement for inflation is that it has to end. In this chapter I will demonstrate how an epoch of early accelerated expansion resolves the issues discussed in § 2 in the simplest scenario of a cosmological constant-like acceleration. I will then introduce the dynamics of an expansion driving scalar field and characterize the power spectra produced. I will only consider single field inflation. These models predict perturbations to be Gaussian, isotropic, and adiabatic, all of which are consistent with observation today.

3.1 SOLVING FLRW PROBLEMS

3.1.1 Accelerated Expansion

Accelerated expansion is easily demonstrated for a Universe dominated by a cosmological constant that is representative of a constant background energy density, Ω_Λ. In this case matter and radiation contributions are negligible (i.e. $\Omega_M, \Omega_R \approx 0$). The Freidmann equation, Eq. (2.9), simplifies to

$$H = \Omega_\Lambda^{1/2} H_0, \tag{3.1}$$

which is a constant. Recall that $H = \frac{\dot{a}}{a}$. Differentiating to find the acceleration of the scale factor yields

$$\frac{\ddot{a}}{a} = \Omega_\Lambda H_0^2 = H^2. \tag{3.2}$$

Thus $\ddot{a} > 0$; the expansion of the Universe is accelerating. The scale factor as a function of time takes the exponential form

$$a(t) = a_i e^{H(t-t_i)}, \tag{3.3}$$

where a_i and t_i are the initial scale factor and time at the onset of this phase of acceleration. Because H is constant (or close to it) during accelerated expansion, we can use the number of e-foldings of expansion as a time analog given by the relation:

$$\frac{dN}{dt} = -H. \tag{3.4}$$

Here the negative represents the fact that we are counting down toward the end of the accelerated phase.

How are horizons behaving? The physical (proper) horizon is still growing at the speed of light, this hasn't changed. But what about the comoving horizon? Recall that in units of $c = 1$, the comoving horizon and the conformal time are interchangeable. The comoving horizon (and conformal time) will evolve according to

$$d\tau = \frac{dt}{a(t)} \tag{3.5}$$

$$= \frac{1}{a_i} e^{-Ht} dt. \tag{3.6}$$

Integrating starting at some initial time we find

$$\tau = -\frac{1}{a(t)H}. \tag{3.7}$$

There is a striking implication to Eq. 3.7. As the cosmological clock moves forward, the conformal time decreases. This behaves similarly to the number of e-foldings: we are counting back to the end of our accelerated phase. Because the conformal time and the comoving horizon are analogously interchangeable, this also reveals that the comoving horizon size is

shrinking! So the physical horizon is growing at the speed of light, but points in space are being driven apart so rapidly that they are overtaking the growth of the physical horizon making their causally connected realms shrink. This is where we shall find the solution to our woes.

3.1.2 Dilution of Monopoles

We have already discussed how our lack of observation of massive magnetic monopoles is in conflict with particle theory's prediction of their existence. If monopoles were produced $\mathcal{O}(1)$ per Hubble volume, and inflation lasted for $N \sim 60$ e-foldings (for reasons to be briefly discussed later). The number density of monopoles would dilute by a factor of $\sim e^{180}$ during inflation! True the horizon began growing again after inflation, however in a matter dominated Universe, for example, when $H_0 = 67.7$ km s^{-1} Mpc^{-1} and $\Omega_M \approx 0.3$, it would take $\approx 6 \times 10^{24}$ Gyrs for the comoving horizon to grow 60 e-foldings. So it would take this long to return to having roughly 1 monopole in the Hubble Volume. So where are all the monopoles? They were blown away.

3.1.3 Solving the Flatness Problem

As discussed in § 2.3.2, the Euclidean spacial geometry of the Universe seems to be strangely particular. Recall that the curvature density can be represented at any time by $\Omega_k = 1 - \Omega$, where Ω is the total energy density of matter, radiation, and dark energy at some time of interest. Using the continuity equation and the Freidmann equation (Eq. (2.5) and (2.8)), it can be shown that [52]

$$\frac{d|\Omega - 1|}{d \ln a} = (1 + 3w)\Omega|\Omega - 1|, \tag{3.8}$$

where w is again the equation of state parameter. This lets us examine the behavior of curvature with respect to the scale factor depending on the domination epoch.

For periods of matter or radiation domination, the equation of state parameter would be $w = 0$ and $w = 1/3$ respectively. During these times Eq. (3.8) results in

$$\frac{d|\Omega - 1|}{d \ln a} > 0. \tag{3.9}$$

Therefore curvature increases (positively or negatively) as the scale factor grows unless the initial condition is the perfectly balanced instability of flat.

For periods of constant energy density with $w = -1$, we find

$$\frac{d|\Omega - 1|}{d \ln a} < 0. \tag{3.10}$$

The curvature is decreasing. This is exactly what has been happening recently during this period of dark energy domination, but it is also our means to arrive at flatness by inflation. Inflation can provide an extended period of accelerated expansion. Without having an estimate on an initial condition for curvature nor a restriction on the total number of e-foldings that took place during inflation, there are no limits as to how much inflation could have flattened the Universe before it ended.

3.1.4 Solving the Horizon Problem

As discussed briefly in § 2.3.3, widely separated patches on the sky have the same temperature. Perturbations that do exist show correlations at large angular scales. In standard cosmology there is no way that they could have been in causal contact at any time in cosmic history. That being the case, they could never have equilibrated to a common temperature nor communicated to have said correlations. One explanation is that the initial condition of the Universe was smooth with preexisting small fluctuations. This is not the only possibility.

Using the Freidmann equation, Eqs. (2.8) and (2.9), and selecting a comoving length scale λ, a relationship between the comoving length, horizon, and curvature is found to be

$$\left(\frac{\lambda}{d_H}\right)^2 |\Omega - 1| = constant. \tag{3.11}$$

Differentiating and utilizing Eq. (3.8), we find

$$\frac{d}{d \ln a}\left(\frac{\lambda}{d_H}\right) = -\frac{1}{2}\left(\frac{\lambda}{d_H}\right)\Omega(1 + 3w). \tag{3.12}$$

All terms except $\frac{d}{d\ln a}\left(\frac{\lambda}{d_H}\right)$ and $(1+3w)$ are positive-definite. Any $w < -1/3$ results in negative pressure and positively accelerated expansion (see Eqs. (2.6) and (2.8)). For $w > -1/3$ we have a decelerated expansion. From Eq. (3.12) we find

$$\frac{d}{d\ln a}\left(\frac{\lambda}{d_H}\right) < 0; \quad w > -\tfrac{1}{3} \tag{3.13}$$

$$\frac{d}{d\ln a}\left(\frac{\lambda}{d_H}\right) > 0; \quad w < -\tfrac{1}{3}. \tag{3.14}$$

So when the equation of state is such that expansion is slowing, comoving length scales are growing slower than the comoving horizon and these lengths are *entering*. This is the case for matter or radiation domination. When the equation of state results in an accelerate expansion, the ratio of comoving lengths and horizon is increasing. Therefore comoving lengths are growing faster than the horizon, and these lengths are *exiting* the horizon. This suggests that if there was an extended period of accelerated expansion at early times, more space was in causal contact at early times before being driven out of communication. Comparing the comoving horizon size at last scattering (the CMB) to the comoving separation of points on opposite sides of the sky, we can estimate that at least 60 e-foldings of inflation were necessary for those points to have been in contact at some time in the past (see [36] where entropy is used to argue this point).

3.1.5 The Perturbation Problem: A Heuristic Solution

Section 2.4 introduced ΛCDM's inability to explain the generation of the small Gaussian, adiabatic anisotropies and inhomogeneities that lead to the formation of structure and are observed in the CMB. In this section I present a heuristic solution offered by inflation. This is an important part of this work, so more attention will be devoted to it later in this chapter.

The solution to the perturbation question is linked to that of the horizon problem in § 3.1.4. The selection of λ to represent comoving length scales was intentional, as it can also represent wavelengths of perturbations. If we consider fields well within the horizon (including photons, density, and even gravity), they may experience quantum fluctuations that are Gaussian, adiabatic, homogeneous, and isotropic. During inflation they are redshifted to classical lengths and driven to superhorizon scales. Henceforth they are frozen.

As they reenter the horizon after inflation ends, they become observable and recommence their evolution. Inflation thus generates the classical perturbations that we observe by driving quantum fluctuations to classical scales and beyond the horizon, preserving them from equilibrating into non-existence before returning to our causal realm.

3.2 DYNAMICS OF SCALAR FIELD INFLATION

Now that we have discussed how inflation solves the problems of the standard cosmological model, we need to address the way to end inflation. By driving inflation with a scalar field, we establish a viable mechanism. I will only consider a minimally coupled single field for two reasons: 1. these are the simplest models and 2. Multi-field models can be phenomenologically represented under a single field. I am also only considering flat spacetimes.

Using the FLRW metric in the form

$$g_{\mu\nu} = \begin{pmatrix} 1 & & & \\ & -a^2(t) & & \\ & & -a^2(t) & \\ & & & -a^2(t) \end{pmatrix}, \tag{3.15}$$

where $\mu, \nu = 0, 1, 2, 3$, the Lagrange density of a scalar field having potential $V(\phi)$ can be written as

$$\mathcal{L}_\phi = \frac{1}{2} g^{\mu\nu} \partial_\mu \phi \partial_\nu \phi - V(\phi). \tag{3.16}$$

We can find the equation of motion for the field ϕ by minimizing the action,

$$S = \int dx^4 \sqrt{-g} \mathcal{L}. \tag{3.17}$$

We find the equation of motion to be

$$\ddot{\phi} + 3H\dot{\phi} - \nabla^2 \phi + \frac{\partial V(\phi)}{\partial \phi} = 0, \tag{3.18}$$

where overdots represent derivatives with respect to cosmological time. If we assume a locally homogeneous scalar field, sufficient inflation will drive this to span the entire Hubble volume. Therefore it is safe to state $\nabla^2\phi \approx 0$. Eq. (3.18) then simplifies to

$$\ddot{\phi} + 3H\dot{\phi} + V'(\phi) = 0. \tag{3.19}$$

Notice that the $3H\dot{\phi}$ term acts as drag. It is this term that supplies energy to the expansion of the Universe. Our assumption of $\nabla^2\phi \approx 0$ does not account for small perturbations in ϕ, which is the subject for § 3.4.1.

If we use the stress-energy tensor for a scalar field

$$T_{\mu\nu} = \partial_\mu\phi\partial_\nu\phi - g_{\mu\nu}\mathcal{L}_\phi, \tag{3.20}$$

and recall for a that for a perfect fluid with pressure p and density ρ as in Eg. (2.4), we find

$$\rho = \frac{1}{2}\dot{\phi}^2 + V(\phi) \tag{3.21}$$

$$p = \frac{1}{2}\dot{\phi}^2 - V(\phi). \tag{3.22}$$

Substituting these in the Freidmann equation, Eq. (2.8), yeids

$$H^2 = \frac{8\pi}{3m_{pl}^2}\left[\frac{1}{2}\dot{\phi}^2 + V(\phi)\right]. \tag{3.23}$$

Defining a new parameter to represent the equation of state [52]

$$\epsilon \equiv \frac{3}{2}\left(\frac{p}{\rho} + 1\right) = \frac{4\pi}{m_{pl}^2}\left(\frac{\dot{\phi}}{H}\right)^2, \tag{3.24}$$

the Raychaudhuri equation (see Eq. 2.8) becomes

$$\frac{\ddot{a}}{a} = H^2(1 - \epsilon). \tag{3.25}$$

Here ϵ describes the speed of ϕ with respect to the expansion rate. Note that according to Eq. (3.25) when $\epsilon < 1$, the universe is undergoing accelerated expansion, and when $\epsilon = 1$, acceleration halts. This is the moment inflation ends. Having a means to end is critically important. Without it, the Universe would eternally exponentiate, and all points in space

would eventually become causally disconnected. The definition provided in Eq. (3.24) also enables us to rewrite the number of e-foldings, Eq. (3.4), as

$$N = -\int H dt = -\int \frac{H}{\dot{\phi}} d\phi = \frac{2\sqrt{\pi}}{m_{pl}} \int \frac{d\phi}{\sqrt{\epsilon}}. \tag{3.26}$$

Using the Freidmann equation above, Eq. (3.23), and the definition of ϵ, Eq. (3.24), it can be show that

$$\epsilon = -\frac{d \ln H}{d \ln a} = \frac{1}{H}\frac{dH}{dN} \tag{3.27}$$

$$H \propto e^{\epsilon N}. \tag{3.28}$$

Finally, we can also include a parameter that describes the acceleration of the field with respect to the drag term in the equation of motion (Eq. (3.19)) [52]:

$$\eta = -\frac{\ddot{\phi}}{H\dot{\phi}} = \epsilon + \frac{1}{2\epsilon}\frac{d\epsilon}{dN}. \tag{3.29}$$

The use of ϵ and η simplify our descriptions of the behavior of the field during its evolution and we will use them extensively.

In summary, I have demonstrated how a scalar field can produce a period of accelerated expansion. I have also shown how the dynamics of a scalar field produce an end to inflation. The formalism and parameterization established will also simplify our descriptions. In the next section, § 3.3, I will illustrate the standard simplified scenario where the field potential dominates the energy ($\dot{\phi}^2 \ll V(\phi)$) and the acceleration in the equation of motion is negligible ($|\ddot{\phi}| \ll 1$). This is commonly referred to as the *slow-roll approximation*.

3.3 SLOW-ROLL

In order to obtain a significant number of e-foldings, the Universe needs to have a phase where the field evolves slowly. In such a state, the energy density will be dominated by the field's potential, and its acceleration will be negligible:

$$\frac{1}{2}\dot{\phi}^2 \ll V(\phi) \tag{3.30}$$

$$|\ddot{\phi}| \approx 0. \tag{3.31}$$

These are referred to as the slow-roll conditions. Such a state of evolution is necessary to a certain degree, otherwise inflation would end too quickly before producing the properties of our observable Universe.

During slow-roll we can see from the equation of motion, Eq. (3.18, that

$$3H\dot{\phi} \approx -V'(\phi); \tag{3.32}$$

the drag term is balanced with the slope of the potential. Without an already existing acceleration, the field cannot establish an acceleration and thus can maintain an extended period of inflation. Granted this is unfavorable because we need inflation to end, but recall that we are only *approximating* that $\ddot{\phi} \approx 0$. There will in fact be a small amount of acceleration that will grow over time, letting the speed of the field build, and thus eventually end inflation. Even though the slow-roll approximation does not suitably describe the evolution as inflation comes to an end, it is a functioning descriptor during the extended period of slow evolution. From Eq. (3.31) we can see that deep into slow-roll $\dot{\phi}^2 \approx 0$, impying that $\dot{\phi} \approx zero$. This then extends to Eq. (3.32) such that $V'(\phi) \approx 0$ making the potential very close to flat. Please note that these are approximate statements intended to illustrate the extreme behaviors during slow roll.

If we consider the Freidmann equation, Eq. (3.23), we see that during slow-roll, the expansion rate of the Universe is governed solely by the potential of the field:

$$H^2 \approx \frac{8\pi}{3m_{pl}^2}V(\phi). \tag{3.33}$$

The above approximations suggest that deep in slow-roll when the potential is approximately constant, so the Hubble parameter is as well. In this situation, then, expansion behaves as though driven by a cosmological constant. Thus the scale factor grows exponentially,

$$a \propto e^{Ht} = e^{-N}. \tag{3.34}$$

As the field approaches the minimum of the potential, slow-roll approximations are no longer valid. Eqs. (3.33) and (3.34) do, however, illustrate an important quality: expansion is no longer driven by the potential. Inflation is over.

Using the equation of motion and the Freidmann equation during slow-roll (Eqs. (3.32) and (3.33)), epsilon takes on a new form:

$$\epsilon \approx \frac{m_{pl}^2}{16\pi}\left(\frac{V'}{V}\right)^2. \tag{3.35}$$

The number of e-foldings between some ϕ and ϕ_* at the end of inflation is

$$N \approx -\frac{8\pi}{m_{pl}^2}\int_{\phi}^{\phi_*}\frac{V}{V'}d\phi, \tag{3.36}$$

as follows from Eq. (3.26). From Eq. (3.29) we can also write the acceleration parameter:

$$\eta \approx \frac{m_{pl}^2}{8\pi}\left[\frac{V''}{V} - \frac{1}{2}\left(\frac{V'}{V}\right)^2\right]. \tag{3.37}$$

In this context ϵ and η are referred to as the *slow-roll paramters*. As both V and H are approximately constant, we can simply define ϵ and η in terms of H instead of V, converting via Eq. (3.33). This is the convention used in § 5.

During slow-roll we can fully characterize the evolution of the field and the expansion rate of the Universe using the slow-roll parameters, the Hubble parameter, and/or the potential. We unfortunately do not know the potential driving inflation, but the predictions from a given model can be tested by observation. In § 5 I discuss how observational constraints can be used to identify the evolutionary history and potential throughout ~ 40 e-foldings of expansion without the assumption of specific models, but next we need to discuss how inflation generates perturbations.

3.4 GENERATING PERTURBATIONS: A CLOSER LOOK

3.4.1 Production

In § 2.4 and § 3.1.5 I reviewed the observed, seemingly coincidental presence anisotropies in the Universe and qualitatively described how an early period of accelerated expansion resolves this issue. Now let us further explore perturbation production (and preservation) by inflation.

If we consider a free scalar field, ψ, that is decoupled from the metric, it behaves as a spectator field and does not effect the evolution of the Universe. Note that this scalar field is not the one driving inflation as discussed previously. Such a scalar field can represent density or gravitational perturbations. I will be working in terms of conformal time (see Eq. (2.11), and their derivatives will be noted with overdots. This is not to be confused with cosmological time derivatives. Let us also continue to assume the presence of a flat FRLW metric.

Because the field of interest is decouple and free, the Lagrange density takes the simple form

$$\mathcal{L} = \frac{1}{2} g^{\mu\nu} \partial_\mu \psi \partial_\nu \psi. \tag{3.38}$$

We can rewrite the metric conveniently as

$$g_{\mu\nu} = a^2(t) \eta_{\mu\nu}, \tag{3.39}$$

where

$$\eta_{\mu\nu} = \begin{pmatrix} 1 & & & \\ & -1 & & \\ & & -1 & \\ & & & -1 \end{pmatrix}, \tag{3.40}$$

is the Minkowski metric describing a static Eucliean spacetime. By writing the metric in this way, we can work in terms conformal temporal elements and comoving spacial elements.

Minimizing the action having the Lagrangian in Eq. (3.38), we arrive at the equation of motion for our field perturbation:

$$\ddot{\psi} + 2\frac{\dot{a}}{a}\dot{\psi} - \nabla^2\psi = 0. \tag{3.41}$$

Fourier expanding ψ makes the equation of motion become

$$\ddot{\psi}_k + 2\frac{\dot{a}}{a}\dot{\psi}_k + k^2\psi = 0, \tag{3.42}$$

where k is the *comoving* wavenumber (momentum state, or frequency, whichever you prefer) such that

$$k_{phys} = \frac{k}{a}. \tag{3.43}$$

For simplicity and as the end result will be directionally independent, we only need to consider its magnitude.

A field redefinition (as shown, for example, in [52])

$$u_k \equiv a\psi_k \tag{3.44}$$

transforms the Fourier space equation of motion, Eq. (3.42), into the Klein-Gordon equation,

$$\ddot{u}_k + \left[k^2 - \frac{\ddot{a}}{a}\right] u_k = 0. \tag{3.45}$$

For modes far outside or deep within the horizon, the resulting mode evolution can be easily shown. Note that these solutions do not account for any evolution *during* horizon crossing.

For extremely long wavelength (small frequency) modes such that $k \ll \ddot{a}/a$, the Klein-Gordon equation (Eq. (3.45)) simplifies enormously to

$$a\ddot{u}_k = \ddot{a}u_k. \tag{3.46}$$

The solution has the trivial form $u_k \propto a$. Recalling our redefinition of our field in Eq. (3.44), the resulting perturbation amplitude $\psi_{\mathbf{k}} = \mathbf{constant}$. So for modes well *outside* the horizon, perturbations are "frozen", no longer evolve, and are preserved until they return to causal connection.

In the opposite extreme, short wavelength modes have $k \gg \ddot{a}/a$, and the Klein-Gordon equation, Eq. (3.45), becomes a standard harmonic oscillator:

$$\ddot{u}_k + k^2 u_k = 0. \tag{3.47}$$

The solution has the form

$$u_k(\tau) = \frac{1}{\sqrt{2k}} \left(A_k e^{-ik\tau} + B_k e^{ik\tau} \right), \tag{3.48}$$

where τ is conformal time and k is the comoving wave number.

We can make this example even more illuminating if we consider the slow-roll condition that $\epsilon \approx constant$. Considering $a \propto e^{-N}$ and $H \propto e^{\epsilon N}$ and recalling Eqs (3.4) and (2.11) for the number of e-folds before the end of inflation and conformal time, respectively, the Raychaudhuri equation, Eq. (2.8), can be written in the form [52]

$$\frac{\ddot{a}}{a} = (aH)^2(2 - \epsilon). \tag{3.49}$$

Now we can rewrite the Klein-Gordon equation, Eq. (3.45), as

$$\ddot{u}_k + \left[k^2 - (aH)^2(2 - \epsilon) \right] u_k = 0; \tag{3.50}$$

Recall that the overdots are derivatives with respect to conformal time and we are working in terms of comoving wavenumbers. It can also be shown that

$$\tau = \left(\frac{1}{\epsilon - 1} \right) \left(\frac{1}{aH} \right), \tag{3.51}$$

enabling Eq. (3.50) to take the form of a Bessel equation [52]:

$$\tau^2(1 - \epsilon)^2 \ddot{u}_k + \left[(k\tau)^2(1 - \epsilon)^2 + (\epsilon - 2) \right] u_k = 0. \tag{3.52}$$

The solutions to Eq. (3.52) take the form

$$u_k = \sqrt{-k\tau} \left[A J_\nu(-k\tau) + B Y_\nu(-k\tau) \right], \tag{3.53}$$

where

$$\nu = \frac{3 - \epsilon}{2(1 - \epsilon)} \tag{3.54}$$

and J_ν and Y_ν are Bessel functions of the first and second kind, respectively.

To see the meaning of this result more clearly, let us consider the case of a pure de Sitter, exponential expansion with $\epsilon = 0$, corresponding to a Bessel index of $\nu = 3/2$. Our solution now appears as

$$u_k = \left(\frac{k\tau - i}{k\tau}\right)\left[Ae^{ik\tau} + Be^{-ik\tau}\right]. \tag{3.55}$$

As we saw previously in Eq. (3.48), modes well within the horizon (large k) behave as harmonic oscillators. Looking at Eq. (3.55), we return to the same conclusion. (As we should!). For high frequency modes, the metric should approach a static, flat Minkowski space, referred to as a Bunch-Davies vacuum. In such a case, vacuum state boundary conditions and quantization normalization specify our solutions in Eq. (3.55) to be [53, 52]

$$u_k = \frac{1}{\sqrt{2k}}e^{ik\tau}. \tag{3.56}$$

The normalized short wavelength solution in Eq. (3.56) provides us with the normalization of the general solution:

$$u_k = \frac{1}{\sqrt{2k}}\left(\frac{k\tau - i}{k\tau}\right)e^{ik\tau}. \tag{3.57}$$

Let us check to see whether the long wavelength solution matches our previous result above (which was a constant). For long wavelength modes that are well outside the horizon, $k \to 0$. Here Eq. (3.57) becomes

$$u_k \approx \frac{1}{\sqrt{2k}}\left(\frac{i}{-k\tau}\right). \tag{3.58}$$

If we continue with our simplified assumption that $\epsilon = 0$ and recall from Eq. (3.51), we can replace τ to arrive at

$$u_k = \frac{iaH}{\sqrt{2}k^{3/2}}. \tag{3.59}$$

Utilizing our definition $\psi_k \equiv u_k/a$ we see that $\psi = constant$. Specifically

$$\psi_k = \frac{iH}{\sqrt{2}k^{3/2}}, \tag{3.60}$$

Our long wavelength modes are again "frozen." These modes are of central interest as they represent the primordial perturbations that reenter the horizon after inflation and seed structure formation.

The above Bessel function solution is still an approximation. We made the assumption that $\epsilon \approx 0$ and $H \approx constant$ throughout. If this were in fact true, inflation would never end. We also only considered the extreme solutions. Modes continue to evolve as they cross the horizon and transition from evolving within and being fronzen without. A more robust and general approximate solution is obtained via the Wentzel- Kramers-Brillouin (WKB) approximation [54] or establishing a hierarchy of slow–roll–like parameters [55] whose evolution is governed by a system of first order linear differential equations [56, 57]. The later of these methods is applied in § 5.

We can now define the power spectrum to be

$$P(k) \equiv \frac{k^3}{2\pi^2} \left\langle \psi_k^2 \right\rangle . \tag{3.61}$$

In the long wavelength limit when perturbations are superhorizon and letting $\sqrt{\langle \psi_k^2 \rangle} = |\psi_k|$, we have

$$P(k) = \left(\frac{H}{2\pi} \right)^2 . \tag{3.62}$$

Note that this is independent of k, and as long as $H \approx constant$, the spectrum has equal power for all modes. This is the well known Harrison−Zeldovich spectrum [58, 59].

3.4.2 Scalar Perturbations

The generation of perturbations discussed in the previous section, § 3.4.1, is generalized for free decoupled spectator fields. Density perturbations are sourced by perturbations in the inflaton field itself, therefore we cannot treat this case as a fully decoupled field. It is perturbations in ϕ discussed in § 3.2 that lead to the seedling density perturbations, $\delta\rho$. As is done with temperature anisotropies, density perturbations are described as their fractional

departure from the mean, $\delta \equiv \delta\rho/\bar{\rho}$. These density perturbations induce local gravitational fluctuations via the Poisson equation:

$$\nabla^2\Phi = 4\pi G\bar{\rho}a^2\delta, \tag{3.63}$$

where ∇ is a comoving gradient and gives rise to the factor of a^2 on the right hand side. In the Newtonian limit of General Relativity, the local gravitational potential is representative of fluctuations in the metric (FLRW), i.e.

$$ds^2 = a^2\left[(1+2\Phi)d\tau^2 - (1-2\Phi)\delta_{ij}dx^i dx^j\right]. \tag{3.64}$$

Because the scalar inflationary field is sourcing the density perturbations, we need to investigate its behavior in a locally perturbed metric. We can treat the field as a comoving fluid with four-velocity $u^i = 0$ when $i \neq 0$. Thus the fluid four-velocity is just representative of its flow through time. As such $u^\mu\phi_{,\mu} = \dot{\phi}$ in the case of homogeneity. By rewriting the stress-energy tensor in terms of $\dot{\phi}$ and the fluid four-velocity, and using our generalized definitions of density and pressure in Eq. (3.22), we can arrive to the familiar equation of motion of the field (Eq. (3.19)),

$$\ddot{\phi} + 3H\dot{\phi} + V'(\phi) = 0. \tag{3.65}$$

A full derivation can be found in [52].

A linear relation exists between the local gravitational potential perturbation to the metric and the local scalar curvature perturbation, $\mathcal{R}$, the Ricci scalar. The derivation can be found in [60] and results in

$$\Phi = -\frac{3(1+w)}{5+3w}\mathcal{R}, \tag{3.66}$$

where w is the equation of state parameter. These perturbations are what make their way to us as temperature anisotropies in the CMB via the Sachs-Wolfe effect [61].

Let us return to the fluid velocity. Because we are working in the comoving frame and the fluid velocity is time-like, we can equate it to the perturbed time component of the metric,

$$u^0 = \sqrt{1+2A}dt \tag{3.67}$$

where I am using A to represent the perturbation in time. To first order in A this becomes

$$u^0 = (1+A)dt = a(1+A)d\tau. \tag{3.68}$$

Its covariant, conformal derivative (remember this is only temporal) then represents a perturbation in the local Hubble parameter. A very hand wavy simplification of a regular conformal time derivative illustrates this point:

$$\begin{aligned} \frac{du^0}{ad\tau} &= \frac{\dot{a}}{a}(1+2A) && (3.69)\\ &= H(1+2A) && (3.70)\\ &= H + \delta H. && (3.71) \end{aligned}$$

For a much more detailed and proper derivation see [52]. If we only consider long wavelengths outside the horizon (those frozen) and properly perform the covariant derivative, we find that

$$\frac{1}{3}u^0{}_{;0} \approx H\left[1 - A - \frac{1}{aH}\frac{\partial \mathcal{R}}{\partial \tau}\right]. \tag{3.72}$$

This behaves just as a perturbed Hubble parameter.

Recall the definition of the number of e-foldings, Eq. (3.4),

$$N \equiv -\int H dt. \tag{3.73}$$

We can now consider a local number of e-folds N' such that

$$N' = -\int H\left[1 - A - \frac{1}{aH}\frac{\partial \mathcal{R}}{\partial \tau}\right] a(1+A)d\tau. \tag{3.74}$$

To first order in A and $\frac{\partial \mathcal{R}}{\partial \tau}$ it simplifies to

$$\begin{aligned} N' &= -\int (H - \frac{\partial \mathcal{R}}{\partial t})dt && (3.75)\\ N' &= N + R && (3.76)\\ \mathcal{R} &= N' - N. && (3.77) \end{aligned}$$

We can see that the curvature perturbation is simply the difference between the local number and background e-foldings of expansion.

Let us now connect the local curvature fluctuations to the perturbations of the scalar density field. Let

$$\mathcal{R} = \delta N \quad \rightarrow \quad dN, \tag{3.78}$$

and

$$dN = \frac{dN}{d\phi} d\phi. \tag{3.79}$$

It follows that

$$dN = \frac{H}{\dot{\phi}} d\phi \rightarrow \mathcal{R} = \frac{H}{\dot{\phi}} \delta\phi. \tag{3.80}$$

Similar to the definition of the power spectrum in Eq. (3.61), we can write the curvature power spectrum as

$$P_{\mathcal{R}}(k) = \frac{k^3}{2\pi^2} \left\langle \mathcal{R}^2 \right\rangle \rightarrow \frac{k^3}{2\pi^2} \left(\frac{H}{\dot{\phi}} \right)^2 \left\langle \delta\phi_k^2 \right\rangle. \tag{3.81}$$

Letting ψ_k from Eq. (3.60) represent $\psi_k = \delta\phi_k = \frac{iH}{\sqrt{2}k^{3/2}}$ as our perturbed scalar field frozen outside the horizon, we can rewrite the curvature power spectrum as

$$P_{\mathcal{R}}(k) = \frac{H^4}{2\pi\dot{\phi}^2}. \tag{3.82}$$

From our definition in Eq. (3.24) and writing $\dot{\phi}$ in terms of ϵ, we arrive to the standard form of the curvature power spectrum:

$$P_{\mathcal{R}}(k) = \frac{H^2}{\pi m_{pl}^2 \epsilon}. \tag{3.83}$$

This is a scale independent Harrison-Zeldovich spectrum under slow roll. As H and ϵ depart from approximate constants, this spectrum will depart from scale independence. Note that unlike tensor modes which will be discussed in the next section, matter perturbations continue to grow due to gravity while still outside the horizon during radiation and matter domination until the onset of dark energy epoch. Those that reenter during radiation domination stall in growth until matter-radiation equality. Extracting the spectrum generated by inflation requires taking the continued evolution into account. In this work the focus is

on the primordial tensor spectrum, so I refrain from an in depth exploration of the continued evolution of scalar modes. I admit that the above skips over the quantization and full derivation of the curvature perturbations, but the details are not relevant here. For a full and thorough treatment see, e.g., [60, 52].

After all of that, we can finally see the primordial power spectrum of curvature (scalar) perturbations. To summarize, Eq. (3.83) describes the rms amplitude of each k mode of curvature perturbations as generated by inflation. Isotropically and homogeneously distributed perturbations in the inflationary field are stretched to classical scales. These then remain isotropically and homogeneously distributed in the Universe and are Gaussian in nature. Perturbations in the inflationary field seed density perturbations that are directly coupled to curvature perturbations and all species of produced particles, thus they are adiabatic. The temperature anisotropies in the CMB that make their way to us are primarily the result of the Sachs-Wolfe effect as photons climb out of the local gravitational potential.

We can now present the standard parameterization of the power spectrum that establishes constrainable observables. As is typical we can approximate the power spectrum as a power law:

$$P_{\mathcal{R}}(k) = A_s k^{n_s - 1}, \tag{3.84}$$

where A_s and n_s are the amplitude and spectral index, respectively. The index is commonly referred to as the tilt of the power spectrum. Note that A_s has to be scaled to a specific mode which acts as a pivot point to the spectrum. In other words,

$$P_{\mathcal{R}}(k) = A_s|_{k_0} \left(\frac{k}{k_0}\right)^{n_s - 1}. \tag{3.85}$$

We can determine the tilt directly from the power spectrum and find

$$n_s - 1 = \frac{d \ln P_{\mathcal{R}}}{d \ln k}. \tag{3.86}$$

Going beyond a standard power law, we can include variations in the tilt, called the running. This is defined as

$$\alpha_s = \frac{dn_s}{d \ln k}. \tag{3.87}$$

When a mode exits the horizon, its comoving wavenumber is approximately equal to the inverse of the Hubble radius (the horizon) such that $k = aH$. This gives us a connection between derivatives with respect to k and N:

$$d\ln k = d\ln(aH) = \frac{1}{aH}\frac{d(aH)}{dN}dN = (\epsilon - 1)dN. \tag{3.88}$$

After some algebra, considering the definitions of the slow-roll parameters (Eqs. (3.24) and (3.29)), the approximations that $a \propto e^{-N}$ and $H \propto e^{\epsilon H}$, and the link provided above in Eq. (3.88), we find the relation

$$n_s - 1 \approx -4\epsilon + 2\eta. \tag{3.89}$$

We now have a direct connection between a constrainable parameter and those that describe inflation. Constraints from the Planck experiment have resulted in $As = 2.142 \pm 0.0049 \times 10^{-9}$, $n_s = 0.9667 \pm 0.0040$, and $\alpha_s = -0.002 \pm 0.0013$ evaluated at ($k = 0.002$ Mpc^{-1}) at 68% confidence [1].

3.4.3 Tensor Perturbations

In section § 3.4.1 we derived the power spectrum for free decoupled scalar field perturbations. Consider now the longitudinal and transverse polarization state tensor perturbations of the metric to behave as independent scalar fields such that

$$\delta g_{ij} = h_{ij} = \left(\frac{32\pi}{m_{pl}^2}\right)^{1/2}(\psi_+ \hat{e}_{ij}^{+} + \psi_x \hat{e}_{ij}^{\times}), \tag{3.90}$$

where the $+$ and $\times$ states are the longitudinal and transverse states, respectively, and the prefactor is a chosen normalization. Then

$$\left\langle h_k^2 \right\rangle = \frac{64\pi}{m_{pl}^2}\left\langle \psi_k^2 \right\rangle, \tag{3.91}$$

where h_k is the strain amplitude of the tensor perturbations. The tensor power spectrum can be written as

$$P_T(k) = \frac{k^3}{2\pi^2}\left\langle h_k^2 \right\rangle = \frac{64\pi}{m_{pl}^2}\frac{k^3}{2\pi^2}\left\langle \psi_k^2 \right\rangle. \tag{3.92}$$

Using our solution for ψ_k in Eq. (3.60) we find

$$P_T(k) = \frac{16H^2}{\pi m_{pl}^2}. \tag{3.93}$$

Note that as long as $H \approx constant$ during slow-roll, this is also scale independent. As with the scalar spectrum, as H evolves this spectrum will depart from its flat behavior. Also, the tensor power spectrum only depends on H (or by proxy V). Hence primordial tensor perturbations provide a direct link to the expansion history and potential during inflation.

We can parameterize the tensor power spectrum and approximate it as a power law of k so that

$$P_T(k) = A_T k^{n_T}, \tag{3.94}$$

where A_T and n_T are the amplitude and spectral index for the tensor spectrum just as we had for scalars. We also need to scale it to a pivot value k_0 (chosing the same as with $P_\mathcal{R}$ in Eq. (3.85)),

$$P_T(k) = A_T|_{k_0} \left(\frac{k}{k_0}\right)^{n_T}. \tag{3.95}$$

By scaling the scalar and tensor power spectra to the same wave mode, we can introduce a new parameter linking the two spectra,

$$r = \left.\frac{A_T}{A_S}\right|_{k_0} \tag{3.96}$$

referred to as the tensor to scalar ratio. Taking the power spectra in Eqs. (3.93) and (3.83) we can relate r to ϵ and find

$$r = 16\epsilon. \tag{3.97}$$

We can also find the tensor spectral index via

$$n_T = \frac{d\ln P(k)}{d\ln k}. \tag{3.98}$$

Using the link between derivatives with respect to k and N in Eq. (3.88) and Eq. (3.28), we find that

$$n_T = \frac{-2\epsilon}{1-\epsilon} \approx -2\epsilon, \tag{3.99}$$

where the latter approximation is made deep in slow-roll when ϵ is small. As with the scalar spectrum, we can also allow for variability in the tensor tilt, called the running of the spectral index, by defining

$$\alpha_T = \frac{dn_T}{d\ln k}. \tag{3.100}$$

By combining Eqs. (3.97) and (3.99) we arrive at a linear relation between the tensor to scalar ratio and the tensor spectral index, known as the *consistency relation*:

$$r = -8n_T. \tag{3.101}$$

This relation predicts that during slow-roll inflation there is a degeneracy between the amplitude and tilt of the tensor spectrum. If the largest scale anisotropies exited the horizon ≈ 60 e-foldings before the end of inflation while the inflationary field was slowly rolling, confirming constraints of this relation will give strong support to inflationary models. These anisotropies are potentially observable as B-mode polarization states in the CMB. The conversion of gravitational waves into B-modes will not be shown here but can be found in [45, 62]. Current constraints on the tensor-to-scalar ratio are only upper bounds, $r < 0.07$ at 95% confidence, made by the BICEP2/Keck Array [63].

As the gravitational waves are free to propagate unhindered through the Universe as opposed to the complicated baryonic physics that muddy our observations of scalar perturbations, direct detection of the stochastic relic background provides a clear window into the inflationary epoch. However, the redshifting of these perturbations due to the continued expansion of the Universe after modes reenter the horizon still needs to be taken into account.

The observable power spectrum today will be different from the primordial. This can be represented by

$$P(k, t_0) = \mathcal{T}^2(\tau_k)P(k, 0), \tag{3.102}$$

where $P(k, t_0)$ is the tensor power spectrum today, $\mathcal{T}(\tau_k)$ is the transfer function accounting for mode evolution after mode k reenters the horizon, and $P(k, 0)$ is the primordial power spectrum discussed above.

As gravitational waves are only effected by the evolution of the scale factor since crossing back into the causal horizon, the transfer function is simply approximated by the ratio of the scale factor at reentry to the scale factor today:

$$\mathcal{T}(\tau_k) = \frac{a_k}{a_0}. \tag{3.103}$$

Recall that k is the wavenumber of each mode, and the wavelengths are therefore $\lambda = 2\pi/k$. Modes cross back into the horizon when their wavelengths are equal to the horizon size. To find the scale factor as a function of modes k as they reenter, we can perform the integral for the horizon size,

$$\frac{2\pi}{k} = d_H = \int_0^k \frac{da}{a^2 H} \tag{3.104}$$

and invert to find $a(k)$.

Care needs to be taken in pursuit of $a(k)$, as during radiation domination, particles are "freezing-out" and becoming non-relativistic as temperatures drop below roughly their mass. This change in relativistic degrees of freedom causes fluctuations in the growth of the scale factor expressed as

$$a = \left(\frac{g_{*s}(T_0)}{g_{*s}(T)}\right)^{1/3} \left(\frac{T_0}{T}\right), \tag{3.105}$$

where T_0 is the CMB temperature today, T is the temperature of the Universe at some time in the past, and the g_{*s}'s are the number of relativistic degrees of freedom at their corresponding temperatures. This is found by conserving entropy and noting that temperature scales as $1/a$. The number of relativistic degrees of freedom is estimated by [36]

$$g_{*s} = \sum_{i=bosons} g_i \left(\frac{T_i}{T}\right)^3 + \frac{7}{8} \sum_{i=fermions} g_i \left(\frac{T_i}{T}\right)^3, \tag{3.106}$$

where the sums are performed over all species of relativistic bosons and fermions, respectively, T_i is the temperature of those relativistic species, and g_i is the degrees of freedom of each species. With the exception of neutrinos, particles become non-relativistic as they fall out of equilibrium with the photon bath. Therefore the only occasion where $T_i \neq T$ will be for neutrinos after they decouple. Anisotropic stress produced by anisotropies in the neutrino field during freeze-out and free streaming also contributes a $\sim$ 20% to 30% reduction for

modes reentering the horizon during radiation domination [64, 65]. More specifically these are the modes that enter before matter–radiation equality, thus $k > k_{eq} = 0.405$. There is a smooth and rapid decline of this effect during the transition from matter to radiation dominance. These effects can be seen in Fig. 4. Note that the transfer function behaves as k^{-2} for modes that reenter during matter domination, while for those entering during radiation domination it acts as k^{-1}. The features in the range of $k \sim 10^1$ to 10^7 Mpc^{-1} are the result of particle freezing out, or becoming non-relativistic, as the Universe expands and cools. This then alters the expansion rate and subsequently the transfer function. The log-log plotting scale exaggerates these features as described above.

We can now characterize the stochastic background as a dimensionless energy density of gravitational waves:

$$\Omega_{GW} = \frac{1}{\rho_{crit}} \frac{d\rho_{GW}}{d\ln k}, \tag{3.107}$$

where ρ_{GW} is the energy density of the background gravitational waves and ρ_{crit} is the critical density of the Universe today. This quantity is directly related to the tensor power spectrum. Rewriting it in terms of the power spectrum, it becomes

$$\Omega_{GW} = \frac{k^2}{6H_0^2} P(k, t_0) \tag{3.108}$$

$$= \frac{k^2}{6H_0^2} P(k, 0) \mathcal{T}^2(t_k). \tag{3.109}$$

A derivation of this expression can be found in [66, 67], but note that the conventions used are slightly different. An example of a resulting gravitational wave background is provided in Fig. 5. This example includes the transfer function discussed above and it assumes a primordial power spectrum with $r = 0.05$ and an unrealistic constant tilt following the consistency relation.

As discussed in this section, the strength of each mode is directly linked to the expansion rate and the potential driving it during inflation. In § 4 and 5 this will be explored further and exploited. I have neglected to explore the effects of reheating on the spectrum. Reheating is the transition period between inflation and radiation domination when the inflationary scalar field converts into particles that decay and transfer their energy to "reheat" the primordial

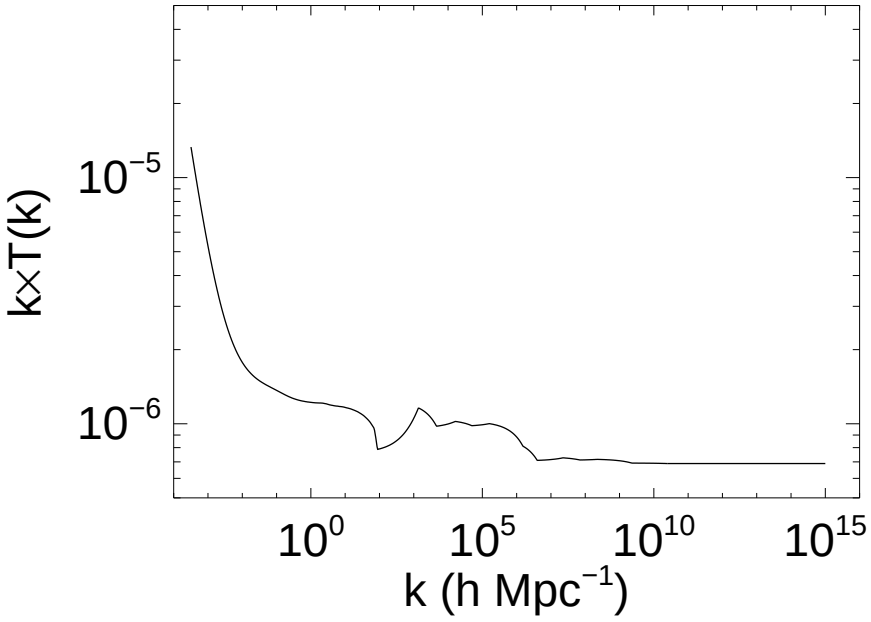

Figure 4: Tensor transfer function which accounts for the evolution of k-modes since reentering the horizon until today. This includes an approximate 20% reduction for modes reentering the horizon during radiation domination. The features between $k \sim 10^1$ and 10^7 Mpc^{-1} are the result of particle becoming non-relativistic as the Universe cools. This in turn affects the expansion rate and therefore the transfer function. The log-log scaling highlight this effect.

plasma [68]. Reheating effects would only become apparent to observations at scales of $k \sim 10^{15}$ Mpc^{-1} if it spanned an extended period of time and finished at $T_{RH} \lesssim 10^9$ GeV [69]. Reheating is an interesting area of study, but in this work I neglect its effects and assume the process was rapid and ended at high temperatures $T_{RH} \sim 10^{15} - 10^{16}$ GeV.

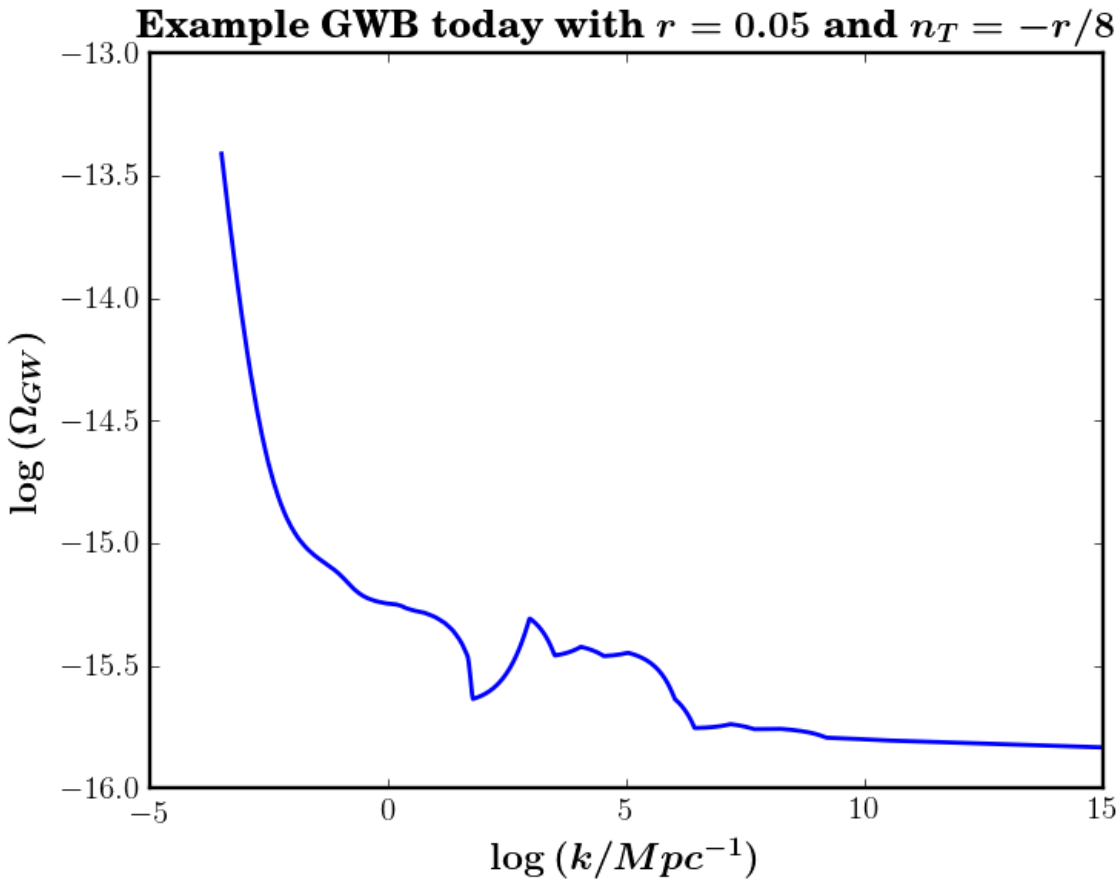

Figure 5: An example gravitational wave background today. This is the unitless gravitational energy density spectrum plotted with a log-log scaling. It assumes a simple constant tilt primordial tensor spectrum with $r = 0.05$ and $n_T = -r/8$.

4.0 TESTING INFLATION WITH THE CONSISTENCY RELATION AND RUNNING OF THE TENSOR SPECTRAL INDEX FROM MULTISCALE MEASUREMENTS

This chapter was published on 16 May, 2014 in *P*hysical Review Letters under the title "Inflationary Tensor Perturbations after BICEP2" with Arthur Kosowsky [70]. It was motivated by the excitement generated by the BICEP2 possible detection of primordial B-mode polarization at a higher than expected amplitude. Of course this was later realized to be, to a significant degree, a result of galactic dust [110, 63].

4.1 INTRODUCTION

The remarkable observations of the BICEP experiment [73], if correct, may reveal the existence of tensor perturbations in the universe with an unexpectedly large amplitude. The measured B-mode component of the polarization power spectrum [42, 43] is consistent with a scale-invariant gravitational wave background with a tensor-scalar ratio of $r = 0.2$. These tensor perturbations could arise from inflation in the early universe, but further characterization of the signal is needed to make this case compelling. The large amplitude of the signal creates a realistic possibility for two independent tests of an inflationary origin for the tensor perturbations: one, higher precision measurements of the B-mode polarization, and two, the direct detection of the gravitational wave background with space-based interferometry. Previous work has considered this pairing of experiments as an inflation probe [74, 75, 76, 77, 78, 79, 80], but their combination becomes far more informative if the amplitude of the tensor perturbations is as large as $r = 0.2$.

Inflation generally produces a power-law power spectrum for both scalar and tensor perturbations, $P_S(k) = A_S\,(k/k_0)^{n_S-1}$ and $P_T(k) = A_T\,(k/k_0)^{n_T}$ (see, e.g., the classic review [81]). The scalar perturbation amplitude A_S and spectral index n_s have been determined to high precision through measurements of the microwave background temperature anisotropies [82, 83, 84]. Thus the amplitude of tensor perturbations is generally characterized by the tensor-scalar ratio, $r \equiv P_T/P_S$, evaluated at the fiducial wavenumber $k_0 \equiv 0.002$ Mpc^{-1}.

The simplest models of inflation, which involve a single dynamical degree of freedom evolving slowly compared to the expansion rate of the universe (single field, slow-roll models) predict a relation between the tensor-to-scalar ratio and the tensor power law index known as the *consistency relation*, $r = -8n_T$ [85]. This connection arises because both the tensor and scalar power spectrum arise from the single degree of freedom. If tensor perturbations with $r = 0.2$ are generated by inflation, the naive expectation is $n_T = -0.025$.

This value for n_T will be observable with anticipated microwave background polarization experiments. Our ability to measure n_T is limited by cosmic variance, which provides a fundamental limit to how well the tensor power spectrum can be measured: we only have a single sky to measure. The cosmic variance of the B-mode polarization power spectrum multipole C_l^{BB} is approximately $\sigma_l = \sqrt{2/(2l+1)f_{\rm sky}}C_l^{BB}$, where $f_{\rm sky}$ is the fraction of the full sky mapped by a given experiment. In addition to tensor perturbations, gravitational lensing of the larger E-mode polarization component will produce B-mode polarization contributing to this cosmic variance [86]. However, with sufficiently sensitive high-resolution polarization maps, the lensing signal can be measured directly using the characteristic non-gaussian distribution of polarization which lensing creates. Knox and Song [87] originally estimated how well the polarization field can be "delensed" using a quadratic maximum-likelihood estimator of Hu and Okamoto [88], finding cosmic variance due to the residual lensing signal of roughly 10% for a perfect sky map. Subsequent work by Hirata and Seljak [89] demonstrated that an iterative application of the quadratic estimator can push delensing significantly further, given maps of sufficient sensitivity and angular resolution. The ability of an experiment with very low noise to measure n_T from a B-mode polarization map will be determined by the cosmic variance from the sum of the primordial tensor signal plus the residual lensing signal after any delensing procedure.

4.2 CONSTRAINING INFLATION VIA THE CONSISTENCY RELATION

Here we estimate the ability of several nominal future polarization experiments to constrain n_T and test the consistency relation (see also [90, 91, 92, 93] for similar estimations of n_T constraints for weaker signals). Sensitivity and angular resolutions of these experiments are given in Table 1; for all cases we assume a sky coverage of $f_{\rm sky} = 0.5$, corresponding to a single ground-based experiment. We assume no foreground contamination or systematic errors; to make these assumptions more believable for a ground-based experiment, we only consider power spectrum measurements with $l > 50$, corresponding to angular scales smaller than 4 degrees. (A detailed foreground study for future polarization satellite missions [94] estimates that, for $r = 0.2$, the tensor B-mode signal will dominate over the foreground B-mode signal for more than 75% of the sky, so the assumption of foreground-cleaned maps from multi-frequency experiments reasonable.) We also assume the theoretical power spectrum of gravitational lensing is known exactly, which will be a good assumption for upcoming experiments based on our knowledge of structure growth in the standard cosmological model. Uncertainties in the lensing model (currently around 2% in the lensing amplitude, e.g. Fig. 12 of [95]) will only cause small changes to these results. We assume the residual lensing signal amplitude given by Seljak and Hirata [89] (listed in Table 1) for the given map sensitivities and angular resolution.

Table 3: Parameters of model polarization experiments.

Experiment	$\sigma_{Q,U}$ (μK-arcmin)	beam (FWHM) (arcmin)	lensing residual [89]
Example A	1.41	4	10%
Example B	0.5	4	5%
Example C	0.25	4	1%

Figure 6 displays allowed values for each experiment in the r-n_T plane, for a fiducial model with $r = 0.2$ and $n_T = -0.025$ satisfying the inflationary consistency relation. These have been calculated using a simple quadratic likelihood evaluated on a grid of models in the

parameter plane. We compute C_l^{BB} using the CAMB package [4] and use only multipoles $50 < l < 2000$ in computing the likelihoods, with a pivot scale $k_0 = 0.002$ Mpc^{-1} . Including higher multipoles has a negligible effect on the likelihoods; the inclusion of lower multipoles also has only a small effect, due to cosmic variance. Improving angular resolution to 2 arcminutes will decrease the lensing residual marginally, by roughly 10% (see Fig. 5 in Ref. [89]). Constraints on n_T improve dramatically as the map sensitivity increases from 1.4 μK-arcmin to 0.25 μK-arcmin, due to better delensing. At the lower sensitivity value, given by Example C, n_T has a normal error of around 0.006, so is measured to be different from 0 at around 4σ. With perfect cleaning of lensing, the significance away from 0 for Example C would increases marginally from 4σ to 5σ, but improving on the residual lensing contribution in Example C requires a more sophisticated treatment of delensing [89]. The same sensitivity and resolution for a full-sky map, presumably from a satellite mission, would increase sky coverage by a factor of 2, decreasing the cosmic-variance limited errors by a factor of $\sqrt{2}$, and give a normal error on n_T of around 0.004, constraining n_T away from zero at a 6σ level.

If the actual amplitude of the tensor perturbations turns out to be $r = 0.1$ instead of $r = 0.2$ (consistent with an alternate foreground dust model in [95]), then the consistency-relation value of n_T decreases by a factor of 2, while the B-mode signal used to measure n_T also decreases in amplitude by a factor of 2. Then a full-sky map with the sensitivity of Example C provides a determination of n_T with error around 0.006, which is now different from 0 at a 2σ significance. The consistency relation still passes a strong test, but we are not able to distinguish between a consistency-relation inflation model and a naive scale-invariant tensor background of unspecified origin.

The example experiments in Table 1 represent a range encompassing possible sensitivities for a so-called "Stage 4" microwave background experiment [96, 97]. The ability to measure n_T depends strongly on the sensitivity in this range. Polarization maps with 4 arcminute resolution or better and map sensitivity of 0.25 μK-arcmin or better can decisively test the inflationary consistency relation between r and n_T for the BICEP value of $r = 0.2$. A measurement of n_T obeying the consistency relation and inconsistent with the generic scale-invariant spectrum $n_T = 0$ would provide highly non-trivial evidence in favor of the tensor perturbations arising from a simple single-field, slow-roll inflation epoch in the early

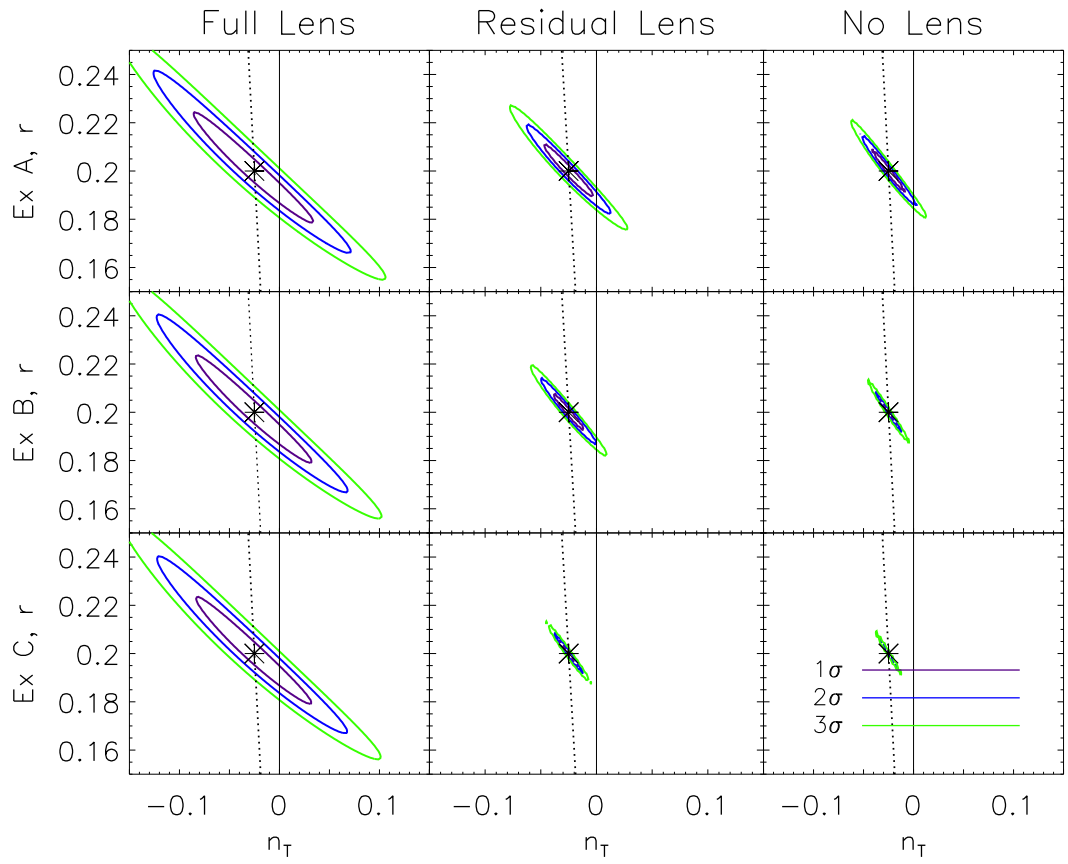

Figure 6: Likelihood countours in the r-n_T plane for the model polarization experiments in Table 1. The fiducial model is $r = 0.2$ and $n_T = -0.025$, indicated by $*$. The dotted line indicates the inflation consistency relation. The vertical line indicates $n_T = 0$ for reference. (Left) Full lensing contribution to the cosmic variance error. (Center) Residual lensing contribution after delensing (see Table 1 for residual lensing noise levels), and (Right) No lensing contribution to the cosmic variance, for comparison.

universe. Note that a value of n_T different from the inflation consistency relation would not necessarily rule out inflation as the source of the tensor perturbations, but could alternately give valuable information that the inflation mechanism was more complicated than a simple slow-roll model, provided the tensor perturbations did arise from inflation.

4.3 B-MODE OBSERVATION AND DIRECT DETECTION OF GRAVITATIONAL WAVES TO CONSTRAIN THE RUNNING OF THE TENSOR SPECTRAL INDEX

The second test of inflation is a direct detection of the tensor perturbations using space-based interferometry. A stochastic background of gravitational waves with a scale-invariant power-law spectrum and an amplitude of $r = 0.2$ results in a tensor energy density of $\Omega_{\rm GW}h^2 \simeq 10^{-15}$. Fortuitously, this tensor amplitude is about the value which maximizes the direct detection amplitude at terrestrial scales [74, 66]. NASA's Big Bang Observer (BBO) concept study [98], an extension of the Laser Interferometer Space Antenna (LISA) proposal to higher sensitivities and shorter satellite separations, would detect this signal at a frequency of 0.1 Hz with a significance of 100σ with one year of observing [99, 100], in the absence of confusion noise from white-dwarf binaries at cosmological distances [100]. Such a binary background will be isotropic with a steeply falling power spectrum; a nonisotropic binary contribution from the Milky Way would also need to be accounted for. A second more speculative stochastic gravitational wave contribution could arise from a possible early-universe phase transition at the electroweak scale [101, 102]. For high-precision characterization of the primordial signal, the competing backgrounds would either need to be modeled with comparable precision, or interferometric measurements would need to have a low-frequency cutoff, reducing the detection significance for BBO substantially [99]. Experiments with greater sensitivity and higher frequency ranges than BBO have been contemplated: Kudoh et al. [99] have calculated that with an 0.2 Hz lower frequency cutoff, their "Fabry-Perot DECIGO" [103, 104] would detect the $r = 0.2$ gravitational wave background at 10σ, while their "Ultimate DECIGO" [105] would detect it at $5 \times 10^4\sigma$.

The B-mode polarization of the microwave background arises from tensor modes with a characteristic wavelength of $k_0^{-1} \simeq 100$ Mpc, while direct detection experiments probe characteristic wavelengths of $c/\nu = 2\times10^{-2}$ A.U., a range covering a factor of 10^{15} in wavelength. A determination of r and n_T in the B-mode power spectrum means that the tensor spectrum can be extrapolated to smaller wavelengths, assuming a perfect power law spectrum. The amplitude at a smaller scale will have an uncertainty governed by the uncertainties in r and

n_T at the larger scale, like those displayed in Fig. 1. If $r = 0.2$, a full-sky B-polarization map with sensitivity below 1 μK arcmin will determine $n_T = -0.025$ with an error of around 0.004. Then extrapolating to a scale 10^{15} times smaller in wavelength using two different values of n_T differing by 0.004 gives an amplitude difference of 20%. This is much larger than the difference due to uncertainty in r which we can ignore.

A direct detection experiment which could measure the tensor amplitude to significantly better than 20% could thus detect a difference from the predicted amplitude with an uncertainty of around 20% of the measured amplitude. Such a difference would arise if the spectrum is not a perfect power law, but rather has some variation in its power law with scale. In analogy with the running of the density perturbation spectrum [106], define the running of the tensor spectral index $\alpha_T \equiv dn_T/d\ln k$. A value of $\alpha_T = 2 \times 10^{-4}$ will result in a difference in amplitude of 20% when extrapolated over a factor of 10^{16} in wavelength; so by comparing with the values of r and n_T measured from B-mode polarization, a direct measurement of the tensor amplitude with interferometry can measure α_T with an error of around 2×10^{-4}. (If $r = 0.1$, then the error on running becomes weaker by about factor of 2.) Discussions of tensor perturbations until now have commonly claimed that any measurement of α_T is hopeless – but we see that it is likely possible to measure the tensor running *better* than scalar running, *if* precise measurements of both r and n_T are obtained from B-mode polarization.

Direct detection of the gravitational wave background with a very high significance, by some future experiment like Ultimate DECIGO, would allow a second measurement of n_T, at a wavelength of around 0.02 A.U. Then this value could be compared with the spectrum extrapolated from the B-mode n_T plus the running required to give the measured amplitude at A.U. scales. Consistency would demonstrate that a constant-running approximation to the tensor power spectrum is valid, and further verify the inflationary origin of this background; in this case, we can hope to have six measured quantities characterizing the physics of inflation (the amplitude, power law index, and running for both scalar and tensor perturbations). If the two values do not match, it would show that further parameters aside from a spectral index and a constant running are required to adequately describe the tensor power spectrum over these scales.

4.4 DISCUSSION

Inflation was invented to solve a well-known litany of cosmological conundrums: the flatness and isotropy of the universe and the absence of magnetic monopoles. Inflation also provides a simple mechanism for generating a primordial gaussian random distribution of nearly scale-invariant density perturbations and phase-coherent acoustic oscillations, which gives an excellent match to observed microwave background temperature anisotropies and the large-scale distribution of galaxies. Aside from these well-observed signals, inflation makes a completely generic prediction of a nearly scale-invariant background of tensor perturbations, which once generated will propagate unimpeded until the present day, and unchanged save for their dilution and stretching due to the expansion of the universe. But the amplitude of this stochastic background depends on the unknown energy scale of inflation. Prior to St. Patrick's Day 2014, we had only suggestive and somewhat controversial theoretical reasons that the tensor amplitude was large enough ever to detect. If the B-mode polarization measured by BICEP is due to inflationary tensor perturbations, their amplitude is a factor of 10 to 100 larger than cautious optimists had hoped. As a result, we suddenly and unexpectedly have within our reach the chance to probe the unknown physics governing the universe at an age of 10^{-36} seconds and an energy scale of 10^{16} GeV, with two completely different experimental approaches. We are surely obliged to try.

5.0 UNVEILING THE INFLATIONARY HISTORY AND POTENTIAL WITH JOINT CONSTRAINTS OF CMB B-MODES AND INTERFEROMETRIC DIRECT DETECTION

This chapter was published in *P*hysical Review D in May 2015 under the title "The History of Inflation from Microwave Background Polarimetry and Laser Interferometry" in collaboration with Arthur Kosowsky (U. Pittsburgh), William Kinney (U. Buffalo), and Naoki Seto (U. Kyoto) [71]. Since the time of publication, new upper bounds on the tensor–to–scalar ratio have been established. The current estimate is $r < 0.07$ at 95% confidence [63].

5.1 INTRODUCTION

The pursuit of comsological B-mode microwave background polarization [42, 43] at large angular scales has seen a burst of attention in the past year since the BICEP2 experiment [73] announced the possibility of a detection in March 2014. Further investigation has revealed that the dominant source of this signal is actually galactic dust [107, 108, 109, 110] rather than being cosmological in nature. This does not rule out the existance of cosmological B-modes, but it is now clear that detecting a cosmological B-mode signal at significantly lower amplitude than the BICEP2 signal requires better characterization of foreground polarization signals via multi-frequency measurements. If we ultimately measure a primordial B-mode signal, it may provide an otherwise unobtainable window into physics at extremely high energies and the evolution of the Universe during its earliest moments.

A period of exponential expansion in the early Universe, known as inflation, resolves several observational difficulties with the standard cosmological model (e.g., [26, 27, 28, 29,

30, 31, 32, 33, 34, 35]). Such a period of expansion can be driven by some component with a nearly constant energy density, such as the potential energy of an effective scalar field (the "inflaton"). During this epoch, quantum fluctuations in the inflaton field are amplified into classical density perturbations which grow by gravitational instability into the structures visible in the Universe today. Likewise, quantum fluctuations in the tensor components of the inflating spacetime are amplified into a stochastic background of gravitational waves, with a nearly scale-invariant power spectrum and an amplitude depending on the energy scale of inflation. Once generated, these tensor perturbations propagate almost freely through the Universe, their wavelengths increased by the expansion of the Universe and their amplitudes decreased by the same factor once the wavelength comes inside the horizon.

The hallmark of an inflationary gravitational wave background is its extremely wide range in wavelengths, roughly from the scale of the horizon today down to terrestrial scales. If inflation occurred when the temperature of the Universe was around the Grand Unification scale of 10^{16} GeV, the gravitational wave background will produce a pattern of B-mode polarization large enough to be seen by upcoming experiments. Remarkably, an inflationary tensor perturbation signal of roughly this amplitude will likely also be detectable directly with future space-based laser interferometers [111, 75, 76, 77, 78, 79, 80, 112, 113, 114]. Direct detection will probe wavelengths that are 15 orders of magnitude smaller than those inducing microwave background signals; measurements at these two scales span a large portion of the observable inflation epoch, and may therefore reveal the physical process driving inflation.Gravitational wave backgrounds of smaller amplitude are more difficult to detect at both cosmological and local scales.

A recent paper showed that an interferometric detection of the inflationary tensor signal will provide qualitatively new information about inflation, namely a precise measurement of any departure from a pure power-law spectrum [70]. If we can obtain information about inflation at widely varying scales, a natural question arises: ultimately, how well can the history of inflation, and the physics driving it, be determined? Here, we determineconstraints on the expansion history during inflation, as well as the corresponding effective potential governing the evolution of the inflaton, from future measurements at both microwave background and interferometer scales. We use a Monte Carlo method to generate random inflation models

with an initially slowly varying inflaton value (the so-called "slow roll" condition) at the time when perturbations on the scale of the horizon today are generated [57, 115] and which satisfy current measurements [110]. Of these models, only a very small fraction satisfy tensor amplitude constraints at the few percent level on both scales, and the resulting expansion histories during inflation are strongly constrained.

Other recent works use similar techniques to constrain inflation. Ref. [116] considers only microwave background measurements; our results show that the additional information from an interferometric detection greatly restricts the range of acceptable inflation models. Ref. [79] focused on detectability of tensor perturbations in specific models by interferometers of a given sensitivity. We extend this work to consider the generic features of inflation models satisfying a particular pair of B-mode polarization and interferometer measurements. Ref. [78] considered models with the largest interferometer signals. We also consider interferometer measurements with sufficient sensitivity to constrain both the amplitude and spectral index of tensor perturbations at local scales, providing additional ability to discriminate between inflationary expansion histories.

5.2 METHODS

We compute the dynamical history and resulting scalar and tensor perturbation spectra for random inflation models chosen via the technique of Monte Carlo inflation flow potential reconstruction [57, 115]. The dynamics of an inflation model can be written in terms of the value of an effective scalar field ϕ (the "inflaton") and its potential energy $V(\phi)$; inflation occurs when the energy density is dominated by the inflaton potential energy. The field ϕ will evolve towards the minimum of the potential as inflation progresses. It is convenient to use the value of the effective inflaton field ϕ during inflation as a time parameter; this can be done as long as ϕ evolves monotonically to smaller values. The Hubble parameter during inflation, $H \equiv (1/a)da/dt$ with $a(t)$ the scale factor, can be used to construct a hierarchy of

"slow-roll parameters" [55]

$$\begin{aligned}
\epsilon &\equiv \frac{m_{\rm Pl}^2}{4\pi}\left(\frac{H'(\phi)}{H(\phi)}\right)^2, \\
\sigma &\equiv \frac{m_{\rm Pl}}{\pi}\left[\frac{1}{2}\left(\frac{H''}{H}\right)-\left(\frac{H'}{H}\right)^2\right], \\
{}^{\ell}\lambda_{\rm H} &\equiv \left(\frac{m_{\rm Pl}^2}{4\pi}\right)^{\ell}\frac{(H')^{\ell-1}}{H^{\ell}}\frac{d^{(\ell+1)}H}{d\phi^{(\ell+1)}}, \qquad \ell \geq 2.
\end{aligned} \tag{5.1}$$

where primes are derivatives with respect to ϕ and the Planck mass $m_{\rm Pl}$ sets the energy units. The evolution of the parameters during inflation is determined by a system of first-order linear equations [56, 57],

$$\begin{aligned}
\frac{d\epsilon}{dN} &= \epsilon\left(\sigma+2\epsilon\right), \\
\frac{d\sigma}{dN} &= -5\epsilon\sigma-12\epsilon^2+2\left({}^{2}\lambda_{\rm H}\right), \\
\frac{d\left({}^{\ell}\lambda_{\rm H}\right)}{dN} &= \left[\frac{\ell-1}{2}\sigma+\left(\ell-2\right)\epsilon\right]\left({}^{\ell}\lambda_{\rm H}\right)+{}^{\ell+1}\lambda_{\rm H}.
\end{aligned} \tag{5.2}$$

In these equations the time variable is the number of expansion e-folds before the end of inflation $N \equiv \ln(a_{\rm end}/a)$ where

$$\frac{d}{dN} = \frac{m_{\rm Pl}}{2\pi^{1/2}}\sqrt{\epsilon}\frac{d}{d\phi}. \tag{5.3}$$

Given a solution for $\epsilon(\phi)$, $H(\phi)$ can be obtained from the definition of ϵ, which then requires normalization given the observed amplitude of the scalar power spectrum [117]. The effective potential $V(\phi)$ then follows from the equation of motion for $H(\phi)$,

$$H^2(\phi)\left[1-\frac{1}{3}\epsilon(\phi)\right] = \frac{8\pi}{3m_{\rm Pl}^2}V(\phi). \tag{5.4}$$

Particular models of inflation are obtained by choosing initial values for the slow-roll parameters; their dynamical evolution corresponds to some trajectory in the slow-roll parameter space. In practice, we truncate the hierarchy Eqs. (5.2) above $\ell = 8$ (corresponding to a restricted subset of exact inflation models) and then evolve the evolution equations until inflation ends, which we take as the condition $\epsilon = 1$. Once the slow-roll parameters are all determined throughout inflation as a function of N, the primordial comoving curvature

perturbation $\delta\rho/\rho$ arising from the scalar perturbations and the tensor/scalar ratio r are, to second-order in the slow roll parameters, given by [55, 118],

$$\begin{aligned} \frac{\delta\rho}{\rho} &\simeq \frac{H}{2\pi m_{\rm Pl}\sqrt{\epsilon}}, \\ r &\simeq 16\epsilon\left[1 - C\left(\sigma + 2\epsilon\right)\right] \end{aligned} \tag{5.5}$$

with $C \equiv 4(\ln 2 + \gamma) - 5 = 0.0814514$, where $\gamma \simeq 0.577$ is Euler's constant, and using the WMAP normalization convention for r [119]. Then the perturbation amplitudes as a function of N can be converted to amplitudes as a function of comoving wavenumber k at the end of inflation by the relation $a(N)H(N) = k$. Generating scalar and tensor perturbations for a random sampling of inflation models is thus reduced to choosing random initial points in the slow-roll parameter space. The resulting primordial scalar perturbation power spectrum $P_S(k) \simeq A_S(k/k_0)^{n_{\rm S}-1}$ and tensor power spectrum $P_T(k) \simeq A_T(k/k_0)^{n_{\rm T}}$ are both approximate power laws on cosmological scales around $k_0 = 0.05$ Mpc^{-1}, with $r \equiv A_T/A_S$.

We initially generate 2×10^4 models within an ellipsoidal parameter space region with principal axes $0.952 < n_{\rm S} < 0.981$ and $0.0 < r < 0.1$; these ranges are consistent with the 95% confidence region from current Planck [117], WMAP polarization [120], and BICEP2/Keck+Planck microwave background measurements [110], as well as baryon acoustic oscillation measurements from the Sloan Digital Sky Survey Data Release 9 [121], the 6dF Galaxy Survey [122], and the WiggleZ Dark Energy Survey [123] (shown in Fig. 5 of Ref. [124]), while the running of the scalar spectral index was restricted to be arbitrarily small ($-0.001 < dn_{\rm S}/d\ln k < 0.001$). Note that the most recent Planck release [1] provides a constraint of $-0.015 < dn_{\rm S}/d\ln k < 0.011$ at 95% confidence. We have not adjusted for this allowed range of values as it will not alter the conclusions of this work and by the time the measurements discussed here are achieved, constraints on $dn_{\rm S}/d\ln k$ will likely be at least as strong as we are considering. For simplicity, parameter degeneracies have not been considered. More specifically, this is done by initially setting $\phi_0 = 0$, $H(\phi_0) = 1$, and randomly selecting $\epsilon \in [0, 0.1]$, $\sigma \in [-0.1, 0.]$, ${}^3\lambda \in [-0.05, 0.05]$, ${}^4\lambda \in [-0.005, 0.005]$, ${}^5\lambda \in [-5 \times 10^{-4}, 5 \times 10^{-4}]$, ${}^6\lambda \in [-5 \times 10^{-5}, 5 \times 10^{-5}]$, ${}^7\lambda \in [-5 \times 10^{-6}, 5 \times 10^{-6}]$, and ${}^8\lambda \in [-5 \times 10^{-7}, 5 \times 10^{-7}]$ with a uniform probability distribution. The models are then

freely evolved to the end of inflation when $\epsilon = 1$. If inflation lasts for the desired 60 efoldings of expansion, the expansion rate is then renormalized to the amplitude of the scalar power spectrum. Those models that produce consistent values of $r, n_{\rm S}$, and $dn_{\rm S}/d\ln k$ at $N = 60$ as stated above are then saved. The full tensor spectrum is then computed by exact numerical evaluation of the mode equation for the cosmological background defined by the selected solution to the flow equations, in place of the slow-roll approximation in Eq. (5.5). The corresponding inflation potential $V(\phi)$ is also computed numerically for each model. Models are not restricted to remain slowly-rolling throughout this evolution (as is appearent in Fig. 7, where models evolve more rapidly and steepen). In particular, toward the end of inflation (low values of N), a departure from slow-roll is required for inflation to come to an end.

We then select the subset of models consistent with tensor amplitudes at cosmological scales corresponding to a fiducial tensor-scalar ratio of $r = 0.05 \pm 0.001$, a precision obtainable by currently anticipated experiments.

Given the tensor perturbation spectrum from a particular inflation model, we obtain the tensor spectrum in the present Universe using well-known techniques for computing the transfer function for the amplitudes and wavelengths [77, 125, 126, 64], assuming the standard ΛCDM cosmology [117]. For simplicity, we assume that the reheating phase after inflation, in which the energy density stored in the kinetic energy of the inflaton field is converted to a thermal bath of relativistic particles, occurs rapidly on a time scale short compared to the Hubble time. We then compute a signal for both B-mode polarization and laser interferometry from the tensor perturbations in each model.

The most recent joint analysis by the Planck and BICEP2/Keck collaborations limit the tensor-scalar ratio to $r < 0.12$ at 95% C.L. [110]. For interferometers, a stochastic gravitational wave power spectrum is often expressed as $\Omega_{\rm GW}(f)$, the fraction of critical density in gravitational waves per unit logarithmic frequency interval. We assume a particular fiducial model of the local tensor perturbations with an amplitude of $\Omega_{\rm GW} = 8.2 \times 10^{-17}$ at a frequency of $f = 0.25$ Hz. We then consider a measurement of this amplitude with a 2σ standard error of around 8%: this corresponds to the reference strain sensitivity $u\sqrt{S_{\rm base}(f)}$ of the DECIGO effective interferometer design given in Fig. 2 of [127], with $u = 1/5$, 3

years of observation, and a low-frequency cutoff of 0.2 Hz to minimize the contaminating astrophysical foreground signal from white dwarf binaries. We also assume perfect removal of neutron star and black hole binary signals. (One interferometer design attaining these specifications comprises four sets of three detectors with optimal sensitivity around 1 Hz. Each group can effectively generate two independent interferometers by taking appropriate combinations of data streams from the set. Pairs of these groups will have overlapping orbits to facilitate correlation analysis. Such an experiment is clearly ambitious, but achievable with known technology at a cost comparable to current large physics and astronomy efforts.) A particular inflation model is considered consistent with the fiducial interferometer signal if its amplitude is within the 2σ range for $\Omega_{\rm GW}$ over the frequency band from 0.2 to 20 Hz.

5.3 RESULTS

Of the 2×10^4 models generated, 568 are consistent with a fiducial cosmological amplitude corresponding to $r = 0.05 \pm 0.001$ for modes that exited the horizon 60 efoldings before the end of inflation. Fig. 7 displays the expansion rate, H, and the effective potential driving the expansion, V, for this subset in violet. The left panels demonstrate the evolution of the expansion rate and potential, respectively, as they are plotted as a function of the time analog representing the number of efoldings before the end of inflation. The right panels show the same quantities as a function of the effective scalar field driving inflation, thus illustrating the physical behavior of the expansion and energy during inflation.

The addition of direct detection constraints by an interferometer further decreases the allowed family of models. A local scale measurement of $\Omega_{\rm GW}(k_0 = 1.6 \times 10^{14}\,{\rm Mpc}^{-1}) = 8.2 \times 10^{-17}$ corresponds to modes that were driven outside the causal horizon approximately 20 efoldings before the end of inflation. Models consistent with this fiducial amplitude within 8% (the 2σ confidence interval for a DECIGO-like experiment with sensitivy scaled by $u = 1/5$ at this fiducial amplitude) are displayed in Fig. 7 in blue. This additional local scale constraint reduces the number of allowed models to 93, 16% of those consistent with the future cosmological constraints and 0.5% of those consistent with current measurements.

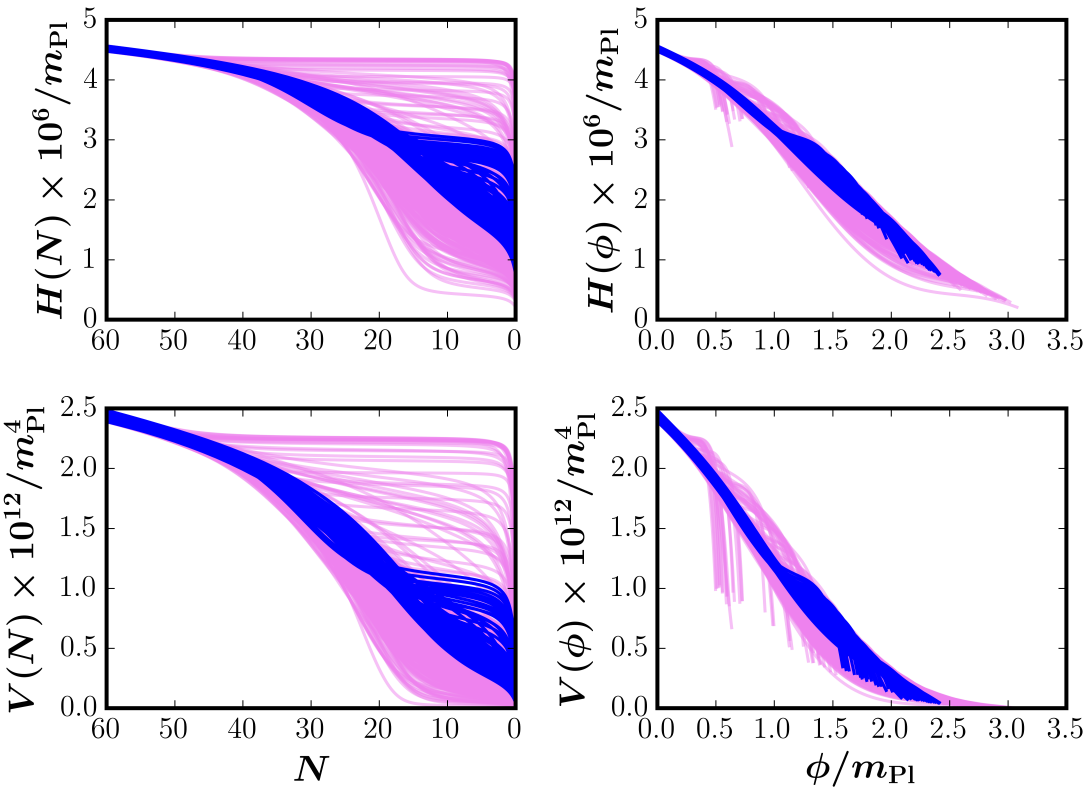

Figure 7: The expansion rates in the form of the Hubble parameter, H, and the effective potentials driving the evolution of the expansion, V, are shown. All models consistent with $r = 0.05 \pm 0.001$ at cosmological scales are plotted in violet. Those models that are also consistent at local scales with $\Omega_{\rm GW}(k_0 = 1.6 \times 10^{14}{\rm Mpc}^{-1}) = (8.2 \pm 0.69) \times 10^{-17}$ are plotted in blue. Note that modes with wave number $k = 1.6 \times 10^{14}{\rm Mpc}^{-1}$ correspond to frequencies $f = 0.25$ Hz. *Right Column*: H and V as a function of the number of efoldings before the end of inflation in the top and bottom panels respectively. *Right Column*: H and V as a function of the effective scalar field, ϕ driving inflation in the top and bottom panels respectively.

Qualitatively, all models consistent with constraints at cosmological and local scales show similar behavior, as illustrated by the blue curves in the left panels in Fig. 7 between $N = 60$ and $N = 20$. A slight increase in the range of model behavior can be seen for $40 > N > 20$, which then translates to a widening of possibilities toward the end of inflation when the fields are departing from slow-roll conditions. Without intermediate and late inflationary epoch constraints on the tensor spectral amplitudes, we can identify properties of the local scale spectrum in order to further constrain the family of models permissible by observation. Specifically, the variety of allowable model amplitudes during intermediate and late time inflationary epochs will also reveal a distribution of spectral tilts, n_T, at local scales. For example, the blue curves in Fig. 7, demonstrate a distribution of spectral tilts, $n_{\rm T}$, for modes with wave numbers of $k = 1.6 \times 10^{14}{\rm Mpc}^{-1}$ that exited the horizon 20 efoldings before inflation ended. This distribution is shown in Fig. 8.

A group of allowed models are clustered around spectral tilts of $n_T = -0.06$ at local scales. The tail in the distribution toward higher values of $n_{\rm T}$ is easily associated with the models in Fig. 7 that fall more rapidly during intermediate epochs and then require a plateauing behavior in order to satisfy the required number of efoldings of expansion. These models all lie below the simpler main group of curves during intermediate times and above toward the end of inflation. These outlying models can be ruled out if interferometric measurements obtained sensitivity levels to constrain the tilt to $n_{\rm T} = -0.06 \pm 0.02$ or better. In order to achieve these constraints at 95% confidence, the previously discussed DECIGO experiment will need a sensitivity level scaling parameter $u = 1/25$, an additional factor of 5 below the strain sensitivity (or a factor of 25 below the sensitivity to $\Omega_{\rm GW}$) used above ($u = 1/5$). This is a factor of 625 increase in sensitivity to $\Omega_{\rm GW}$ beyond the base design for DECIGO.

Applying these spectral tilt constraints to the models consistent at both cosmological and local scales as shown in blue in Fig. 7 (albeit without constricting the constraints on local scale amplitudes), we further reduce the number of consistent models to 78. This subset is illustrated in Fig. 9 in black, plotted over the models shown in Fig. 7. To further illustrate the distribution of each of these subsets of models, Fig. 10 indicates the mean and the band containing 95% of the models about the mean for each family of curves shown

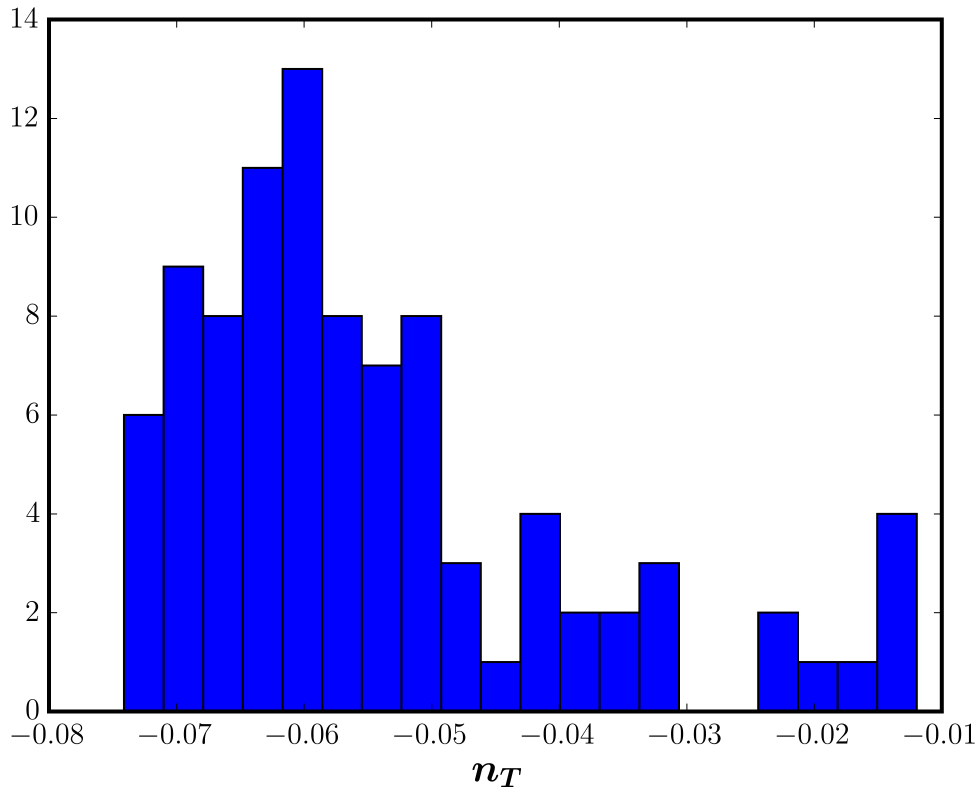

Figure 8: The distribution of spectral tilts of models consistent with cosmological constraints with amplitudes corresponding to $r = 0.05 \pm 0.001$ and at local scales with $\Omega_{\rm GW} = (8.2 \pm 0.69) \times 10^{-17}$ at 95% confidence for modes with wavenumber $k = 1.6 \times 10^{14} Mpc^{-1}$ that exited the horizon 20 efoldings before the end of inflation.

in Fig. 9. Here, the blue curves from Fig. 9 have their mean plotted as blue and the 95% spread of models shown as gray. Similarly for the violet curves from Fig. 9, the mean and 95% spread of models about the mean are shown in Fig. 10 as black and violet respectively. Although this additional constraint has not greatly reduced the number of allowed models, it has significantly restricted the qualitative behavioral forms. If the local scale spectral index were measured to be $n_T = -0.02 \pm 0.02$, only a few models with more complex potential shapes would be consistent.

This conclusion will hold even for a tensor spectrum with a lower amplitude than the fiducially chosen value, provided that the amplitude can still be measured on both scales with similar fractional errors as used here. Of course, the lower the amplitude, the more technically challenging these measurements become. For amplitudes significantly below $r = 10^{-3}$, confusion with the residual gravitational lensing signal will prevent measurement of the tensor amplitude using B-mode polarization [128, 129], while the binary confusion limit becomes an increasing problem for interferometer measurements.

5.4 DISCUSSION

These results clearly demonstrate the capacity of combined measurements of the tensor power spectrum at both microwave background and interferometric scales to constrain the history and physics of inflation. The family of inflation models consistent with both measurements is vastly restricted compared to inflation models consistent only with an amplitude measurement at a single scale. Furthermore, the combined measurements determine the inflaton potential and expansion history over a wide range of field values and evolutionary epochs. We have assumed B-mode polarization measurements of the tensor amplitude with precision at the $r = 0.001$ level; upcoming polarization experiments with increased sensitivity and frequency coverage are expected to surpass this (see, e.g., [130]). We also assume a future interferometer measurement of the tensor amplitude at the 8% level, which will be challenging but feasible if there is in fact a measureable cosmological tensor signal. Pushing the sensitivity of interferometric experiments farther opens the possibilty of further restrict-

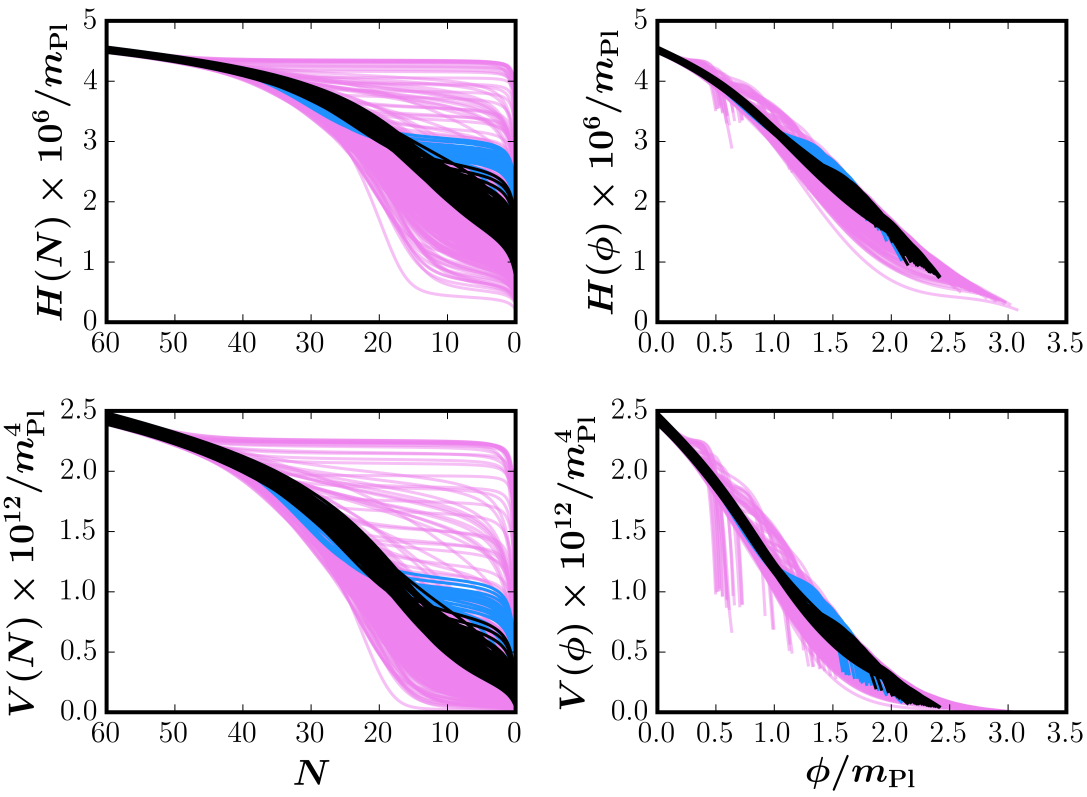

Figure 9: The same models as shown in Fig. 7. The smaller subset of models that have local scale tensor spectral tilts of $n_{\rm T} \in [-0.08, -0.04]$ are plotted in black.

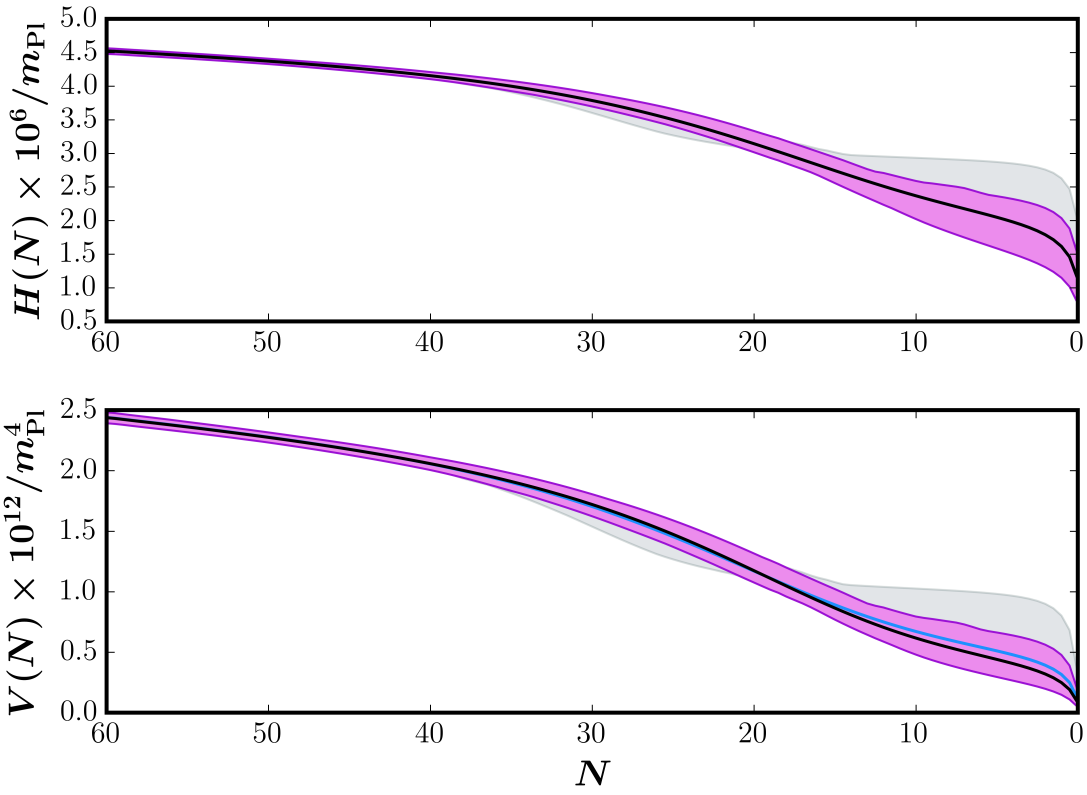

Figure 10: The mean and 95% spread about the mean of models shown in Fig. 9. Here the potentials and expansion rates consistent with $r = 0.05 \pm 0.001$ with 2σ confidence at cosmological scales (corresponding to 60 efoldings before the end of inflation), as well as at local scales (corresponding to 20 efoldings before the end of inflation) with $8\%, 2\sigma$ error on the amplitude have their mean plotted in blue and the spread of models illustrated as a gray band. The set of models that additionally have spectral tilt constraints at local scales in the range of $-0.08 < n_{\rm T} < -0.04$ have their mean plotted in black with their spread about the mean as a violet band.

ing the family of allowed models via the tilt of the spectra at these scales. Clearly such a measurement vastly restricts the behavioral variety of consistent inflationary models.

It may seem surprising that the tilt of the tensor spectrum varies so greatly between scales corresponding to 60 and 20 efoldings before the end of inflation. Recall, however, that during slow-roll $\epsilon \propto (V'/V)^2$, where the prime indicates the derivative with respect to the effective scalar field ϕ and V is the effective potential of that scalar field. As illustrated in Fig. 7 and 9, the potentials drop by a factor of approximately 3 between $N = 60$ and $N = 20$. When plotted as a function of ϕ, this roughly corresponds to the interval of $\phi \in [0.0, 1.0]$. In this interval, the slope of the potential steepens only slightly. Taking both the slight steepening of the slope and the drop in the value of the potential into consideration, we estimate epsilon to increase by a factor of *at least* 9. Our fiducial selection of models at $N = 60$ have amplitudes corresponding to $r = 0.05 \pm 0.001$ and have tilts centered on $n_{\rm T} = -6.25 \times 10^{-3}$ (as to be expected according to the slow-roll consistency relation, $r = -8n_{\rm T}$). Moving to $N = 20$ and increasing ϵ by a factor of roughly 9 then results in a distribution of tilts at these scales to be centered on roughly $n_{\rm T} \approx -0.06$. This is consistent with what we have found in the distribution of tilts at local scales, as illustrated in Fig. 8, and is indicative of the dominance of slow-roll behavior throughout these 40 efoldings of evolution. The outlying models underwent brief departures from slow-roll evolution before returning to ensure the necessary number of efoldings of expansion are completed. This behavior directly translates to the tilt of the spectrum at local scales, thus providing a probe of the expansion history and effective potential driving inflation during epochs corresponding to otherwise unmeasureable scales.

We have made the simplifying physical assumption that reheating after inflation happens quickly, i.e. on a time scale less than a Hubble time, so it has little effect on the expansion history of the Universe. Some models of reheating take significantly longer than this, resulting in a period of matter-dominated expansion prior to the usual radiation-dominated era which can modify the tensor amplitude at small scales (e.g., [131]). Measurements of both the tensor amplitude and the scalar spectral index will give interesting constraints on the duration of any reheating epoch [132]. An extension of the present analysis to include reheating will be considered elsewhere.

The numerical analysis in this paper does not have a rigorous quantification of Monte Carlo coverage of the inflation model space. The truncation of the slow-roll hierarchy at a given order results in only a particular subset of inflation models in the allowed model space. Larger computational efforts can include higher-order truncations, effectively expanding the model space which is explored, and more total models in each Monte Carlo, which will sharpen statistical conclusions. It is unlikely that models not available in our 8th-order slow-roll hierarchy will change our conclusions in a qualitative sense, since the allowed models span a wide range of potentials, as is visible in Fig. 7. However, whether rare successful models exist which are clearly different from the family of models identified here is an interesting open question. These rare cases may be further constrained by additional sources of information.

The results presented here show that a detection of inflationary tensor perturbations at two widely separated scales, the cosmological scale via B-polarization of the microwave background and the Earth-Moon scale via a space-based laser interferometer, will determine the dynamical history of the Universe during the inflation era. In turn, such measurements will give strong constraints on fundamental physics at energy scales of 10^{16} GeV, inaccessible by any other means.

6.0 CONCLUSIONS

Inflation stretches quantum tensor and curvature fluctuations to classical scales. These modes are preserved after being driven beyond the horizon. As such, wavelengths (and frequencies) are tracers of the times when those perturbations exited the horizon, the value of the scalar field ϕ driving expansion, and the number of e-foldings that remain before inflation ends. Perturbation amplitudes on the other hand are directly linked to the expansion rate and the potential of the inflationary scalar field. Measurements of these primordial perturbations across a range in frequencies provide a mapping of the expansion history and the evolution of the potential with respect to N and ϕ. As discuss in § 5, a joint constraint of the amplitude of the primordial tensor power signal at CMB and solar system scales greatly reduces the viable models of potentials and expansion histories during inflation as shown in Fig. 7 of § 5. The addition of intermediate measurements (perhaps at $N \approx 40$) would amplify the constrainability of inflationary histories and the underlying physics therein.

Successfully measuring the primordial tensor power spectrum at any scale is no small task. The excitement generated by the first detection of B-mode polarization by BICEP 2 [95] and the subsequent revelation that the signal is largely due to dust foregrounds [110, 63, 133] is a clear example of that. Dust, sensitivity, and the ever present experimental systematics are the dragons that must be tamed to reach the underlying primordial signal.

Foreground dust produced B-mode polarization must be accurately characterized if a subdominant primordial signal is to be revealed [134]. Efforts are underway to accomplish this. The BFORE mission has been proposed specifically designed to probe the presence of polarization producing galactic dust to supplement existing experiments [135]. With accurate dust modeling, future CMB missions such as Core [136], LiteBIRD [137], PIXIE [130], EPIC [138], and PRISM [139] will have the sensitivity to detect a tensor-to-scalar ratio of $r \sim 10^{-3}$

to 10^{-4}. As is discussed in § 4, missions such as these may even have the ability to measure the tilt of the power spectrum if lensing is accurately taken into account.

The lensing B-mode signal has a significant presence at all scales and peaks at $l \approx 1000$. It is the result of E-modes converting to B-modes as polarized light is deflected by structure on its journey to us [140]. The lensing signal, which will be non-Gaussian, can be estimated using a quadratic estimator formed from a_{lm}'s at different angular scales (different values of l and m) in temperature and polarization [88, 87, 89]. The Atacama Cosmology Telescope (ACT) has successfully estimated the gravitational lensing of the CMB using this method [142]. Using the fact that the cosmic infrared background (CIB) traces structure, the South Pole Telescope (SPT) and ACT have cross correlated the CMB with the CIB to detect lensing as well [141, 143]. Recently the lensing B-mode signal has been detected directly by the BICEP2/Keck experiment for the first time [148]. With high map sensitivity, the effects of lensing can be strongly constrained, giving access to any underlying primordial B-mode signal.

Direct detection of gravitational waves at small scales has significant challenges as well. The Laser Interferometer Gravitational Wave Observatory's (LIGO) recent first detection of gravitational waves due to coalescing black holes [149] is a technological and scientific triumph, giving promise to future experiments. Development of a space based gravitational wave interferometer is the next step. The LISA (Laser Interferometer Space Antenna) Pathfinder experiment, designed to test the sensitivities of the free-fall interferometric technologies needed for full gravitational wave experiments, was a huge success [150]. This paves the way for space based gravitational wave observatories, beginning with the Evolved Laser Interferometer Space Antenna (eLISA) [151]. The success of the first space-based interferometers is critical for missions such as DECIGO to launch and begin their search for the primordial gravitational wave background.

As is the case with the CMB scale primordial tensor perturbations, foreground sources can hide the local primordial signal. At small scales these sources are astrophysical in nature. Some examples are core collapse supernovae and inspiraling and coalescing compact binaries, each of which has a distinct spectral fingerprint. These signals should be roughly isotropic across the sky. Because they span the history of stellar activity in the Universe, they

should be numerous. The superposition of inspiraling compact binary signals will produce an isotropic stochastic background. Burst events by mergers or core collapse supernovae will create a shot noise signal due to their lower event rate, short duration, and signal strength. Bursts that are frequent enough to have a slight overlap in their waveforms can also contribute a "popcorn" background signal. For a visual example of the three types of astrophysical signals, see Fig. 2 of [152]. The non-Gaussian nature of the latter two signals provides a means to distinguish them from any underlying Gaussian spectrum. The first of these three signals is continuous and likely Gaussian, making it a troublesome mask for the primordial signal. Fortunately the compact binary foreground signal has a frequency cut off that can be exploited. The highest frequencies possible will be just before objects merge. White dwarf - white dwarf binaries are likely to contribute a large portion of the stochastic astrophysical background. Their signals will cut off at frequencies of $\sim 10^{-2}$ to 10^{-1} Hz. Thus a frequency window is available $\gtrsim 10^{-1}$ Hz (corresponding to $k \gtrsim 10^{13}$ Mpc^{-1}) where a large portion of the astrophysical contaminant is not present. Future mission such as the Big Bang Observer (BBO) Stage 2 [153] and advanced stages of the DECi-hertz Interferometer Gravitational wave Observatory (DECIGO) [103, 104] may have the sensitivity at these frequencies to constrain the amplitude of the stochastic background of inflationary gravitational waves at solar system scales. This prospective sensitivity was utilized in § 4 and § 5.

Any additional constraints on the tensor spectrum at other scales drastically limit the consistent expansion histories and potentials. Qualitatively, Figs. 9 and 10 suggest that the tilt of the tensor spectrum at local scales is strongly correlated to the properties at intermediate scales for relatively smooth potentials. Intermediate scale observations would potentially confirm or falsify this trait. Intermediate measurements will also reveal the presence or lack of rapid variations. The discovery of such potentials would indicate that the assumptions of smooth, decreasing potentials in the reconstruction technique of § 5 are invalid. Pulsar timing arrays (PTAs) are experiments working at such scales in a frequency range of $f \in [10^{-9}, 10^{-7}]$ Hz (or $k \in [10^{7}, 10^{9}]$ Mpc^{-1}) (e.g. see [154]). Unfortunately even the "optimal" PTA observing over a 20 year period with an array of 200 pulsars would be unable to detect the tensor spectrum at the current upper limits on the tensor-to-scalar ratio $r < 0.07$ [63] with $n_T \leq 0$ in the absence of any unlikely extreme behavior [155, 154].

They would, however, be able to rule out or detect primordial signals that have blue tilts at CMB scales with $n_T > 0$ (see Fig.1 of [154]). In principle intermediate scale measurements with strong constraints would amplify our ability to identify the evolutionary history during inflation across ~ 40 e-foldings of expansion, but PTAs are not likely to provide them.

As used in § 5, measurements of the primordial scalar power spectrum also put restrictions on the allowed inflation models. Currently we have confident measures of the scalar amplitude and tilt from the CMB. The addition of constraints at other scales would put further restrictions. Care must be taken at smaller scales, however, as the power spectrum is in the fully non-linear regime [144]. At scales corresponding to clusters and larger corresponding to $k \in [0.01, 5]$ Mpc^{-1}, LSS sheds some light on the primordial power spectrum [156]. By mapping the galaxy and cluster density field, all sky surveys such as Euclid [157] and the Large Synoptic Survey Telescope (LSST) [158] may provide such constraints. Galaxies and baryonic matter unfortunately may not be exact tracers of dark matter halos. This creates uncertainty in the form of a bias factor which needs to be accounted for in order to confidently arrive at the primordial scalar power spectrum [159, 160]. As discussed above, weak gravitational lensing of background photons provides a tracer of the LSS matter distribution. Measurements of weak lensing thus provide substantial constraints on the power spectrum [145]. This bypasses (and constrains [146, 147]) the bias associated with photometric mapping of structure and gives a clearer window to the matter power spectrum.

There are other more subtle tracers of LSS that can be explore. Before reionization neutral hydrogen was in abundance. Electron spin flips to lower energy states in hydrogen emit light with a wavelength of 21 cm. These emission lines can therefore be used as a tracer of gas overdensities, a proxy to matter and curvature perturbations. Observations can provide constraints on the primordial matter power spectrum for modes with roughly $k \in [0.1, 1]$ [162, 163]. The Hydrogen Epoch of Reionization Array (HERA) [164] and the Omniscope [165] may realize this goal. As is with all observations, foregrounds (natural or human made) will certainly be problematic for these efforts. Along with emission lines, absorption can be exploited. Light emitted from quasars and active galactic nuclei at high redshifts is readily absorbed by intervening hydrogen gas, specifically by the Lyman α transition. On its journey to us, the light encounters many absorbers. The intervening hydrogen clumps are at

different redshifts, creating a "forest" of Lyman α absorption lines in the observed spectrum. This forest thus traces the growth of structure and matter perturbations across a wide range of redshifts, enabling the estimation of the scalar power spectrum of modes $k \in [0.1, 20]$ [166, 167, 168].

On subgalactic scales the detection of subtle effects due to dark matter subhalos can probe the primordial matter power spectrum. Microlensing detections in our own galaxy can be used to constrain the abundance of dark matter subhalos [169]. Dark matter decay and annihilation detections originating from such halos has also been proposed to track their abundances [170, 171]. It may also be possible to utilize precise measurements of galactic dynamics [172] and tidal tail and stream distortions [173, 174] to trace the presence of these halos. Identifying the dark matter subhalos within our galaxy can lead to constraints on the power spectrum on scales corresponding roughly to $k \in [1, 10^4]$ Mpc^{-1}.

Another potential avenue for constraining small scales of the scalar power spectrum is through spectral distortions of the CMB. Perturbations entering the horizon before decoupling are thermally washed away by Silk dampening. The original state of slight disequilibrium, however, results in scattering events that distort the spectrum from a pure blackbody. Such events should take place in the redshift range of $z \approx 10^4$ to 10^6 corresponding to frequencies of $k \approx 10^1$ to 10^4 Mpc^{-1}. These distortions may be detectable by missions like PIXIE due to the large number of frequency channels [175, 176].

Figure 11 summarizes the various experiments and methods to constrain the scalar and tensor power spectra discussed above (i.e.CMB, 21 cm, Lyman α, CMB spectral distortion, LSS and weak lensing, dark matter subhalo mapping by various means, PTAs and space-based interferometric gravitational wave observatories) and their effective frequency bands. Blue and red lines indicate the experiments will constrain the tensor and scalar primordial power spectrum, respectively. The CMB is designate black as it holds the potential to constrain both power spectra. The "Subhalo" label is inclusive of microlensing, dark matter decay and annhiliations, and intragalactic dynamics and tidal stream distortion. Fig. 11 is not intended to represent the relative sensitivity of these experiments; the offsets are merely for clarity.

The direct detection of gravitational waves by LIGO [149], the first measurements of B-

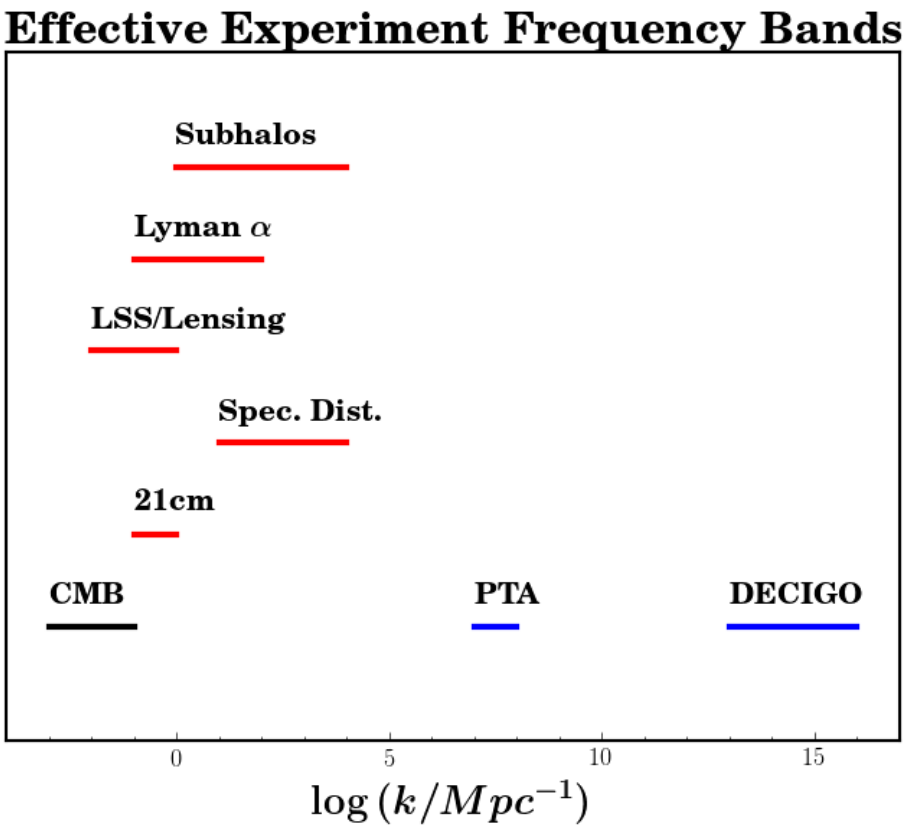

Figure 11: The effective frequency bands of experiments to constrain the tensor and scalar power spectra. Blue (red) lines indicate the experiment will constrain the tensor (scalar) power spectrum. Black is used for the CMB to indicate that it will constrain both spectra. The "Subhalo" label is an umbrella category that includes microlensing, dark matter decay and annhiliations, and intragalactic dynamics and tidal stream distortion. Offsets are for clarity and not to be taken as relative sensitivity.

mode polarization by the BICEP2 experiment [95], and the exceded sensitivity expectations of the LISA Pathfinder mission [150] are not detections of the primordial gravitational relic themselves, but they are vast technological strides on the path to finding it. Future missions may finally reveal this elusive background. Independent measurements will be a great test of the inflationary paradigm. Multiple joint constraints of scalars and tensors at widely separated length scales, however, will hone in on the the expansion history and potential of inflation across roughly 40 e-foldings of evolution. This will not only shed light on the evolution of the Universe when it was between 10^{-36} and 10^{-32} seconds old, but it will also reveal physics at energy scales of $\mathcal{O}(10^{16})$ GeV. These energies are unreachable by Terran particle accelerators. This is an exciting time in cosmology. We are approaching a summit of discovery in our pursuit of the beginning. The view we find will surely be spectacular.

BIBLIOGRAPHY

[1] Planck Collaboration and P. A. R. Ade et al. Planck 2015 results. XIII. Cosmological parameters. arvix:1502.01589, February 2015.

[2] J. C. Mather et al. Calibrator Design for the COBE Far-Infrared Absolute Spectrophotometer (FIRAS). ApJ, 512:511–520, February 1999.

[3] Planck Collaboration and R. Adam et al. Planck 2015 results. I. Overview of products and scientific results. arxiv:1502.01582, February 2015.

[4] A. Lewis et al. Efficient computation of CMB anisotropies in closed FRW models. ApJ, 538:473–476, 2000.

[5] U. Seljak, M. Zaldarriaga, "CMBFAST".

[6] D. Blas, J. Lesgourgues and T. Tram. The Cosmic Linear Anisotropy Solving System (CLASS). Part II: Approximation schemes. J. Cosmology Astropart. Phys., 7:034, July 2011.

[7] E. Hubble. A Relation between Distance and Radial Velocity among Extra-Galactic Nebulae. *Proceedings of the National Academy of Science*, 15:168–173, March 1929.

[8] A. A. Penzias and R. W. Wilson. A Measurement of Excess Antenna Temperature at 4080 Mc/s. ApJ, 142:419–421, July 1965.

[9] F. Zwicky. Die Rotverschiebung von extragalaktischen Nebeln. *Helvetica Physica Acta*, 6:110–127, 1933.

[10] J. H. Oort. The force exerted by the stellar system in the direction perpendicular to the galactic plane and some related problems. *Bull. Astron. Inst. Netherlands*, 6:249, August 1932.

[11] H. W. Babcock. The rotation of the Andromeda Nebula. *Lick Observatory Bulletin*, 19:41–51, 1939.

[12] V. C. Rubin and W. K. Ford, Jr. Rotation of the Andromeda Nebula from a Spectroscopic Survey of Emission Regions. ApJ, 159:379, February 1970.

[13] D. Clowe, A. Gonzalez, and M. Markevitch. Weak-Lensing Mass Reconstruction of the Interacting Cluster 1E 0657-558: Direct Evidence for the Existence of Dark Matter. ApJ, 604:596–603, April 2004.

[14] D. Coe, N. Benítez, T. Broadhurst, and L. A. Moustakas. A High-resolution Mass Map of Galaxy Cluster Substructure: LensPerfect Analysis of A1689. ApJ, 723:1678–1702, November 2010.

[15] C. L. Bennett, D. Larson, J. L. Weiland, N. Jarosik, G. Hinshaw, N. Odegard, K. M. Smith, R. S. Hill, B. Gold, M. Halpern, E. Komatsu, M. R. Nolta, L. Page, D. N. Spergel, E. Wollack, J. Dunkley, A. Kogut, M. Limon, S. S. Meyer, G. S. Tucker, and E. L. Wright. Nine-year Wilkinson Microwave Anisotropy Probe (WMAP) Observations: Final Maps and Results. ApJS, 208:20, October 2013.

[16] G. E. Addison, G. Hinshaw, and M. Halpern. Cosmological constraints from baryon acoustic oscillations and clustering of large-scale structure. MNRAS, 436:1674–1683, December 2013.

[17] M. Viel, J. S. Bolton, and M. G. Haehnelt. Cosmological and astrophysical constraints from the Lyman α forest flux probability distribution function. MNRAS, 399:L39–L43, October 2009.

[18] M. Markevitch, A. H. Gonzalez, D. Clowe, A. Vikhlinin, W. Forman, C. Jones, S. Murray, and W. Tucker. Direct Constraints on the Dark Matter Self-Interaction Cross Section from the Merging Galaxy Cluster 1E 0657-56. ApJ, 606:819–824, May 2004.

[19] LUX Collaboration, D. S. Akerib et al. First results from the LUX dark matter experiment at the Sanford Underground Research Facility. arxiv:1310.8214, October 2013.

[20] J. Hoskins et al. Search for nonvirialized axionic dark matter. Phys. Rev. D, 84(12):121302, December 2011.

[21] D. Hooper and L. Goodenough. Dark matter annihilation in the Galactic Center as seen by the Fermi Gamma Ray Space Telescope. *Physics Letters B*, 697:412–428, March 2011.

[22] A. Einstein. Kosmologische Betrachtungen zur allgemeinen Relativitätstheorie. *Sitzungsberichte der Königlich Preußischen Akademie der Wissenschaften (Berlin), Seite 142-152.*, pages 142–152, 1917.

[23] S. Perlmutter et al. Measurements of Ω and Λ from 42 High-Redshift Supernovae. ApJ, 517:565–586, June 1999.

[24] A. G. Riess et al. Observational Evidence from Supernovae for an Accelerating Universe and a Cosmological Constant. AJ, 116:1009–1038, September 1998.

[25] B. P. Schmidt et al. The High-Z Supernova Search: Measuring Cosmic Deceleration and Global Curvature of the Universe Using Type IA Supernovae. ApJ, 507:46–63, November 1998.

[26] Alan H. Guth. The Inflationary Universe: A Possible Solution to the Horizon and Flatness Problems. Phys. Rev. D, 23:347–356, 1981.

[27] Andrei D. Linde. A New Inflationary Universe Scenario: A Possible Solution of the Horizon, Flatness, Homogeneity, Isotropy and Primordial Monopole Problems. *Phys.Lett.B*, 108:389–393, 1982.

[28] A. Albrecht and P. J. Steinhardt. Cosmology for Grand Unified Theories with Radiatively Induced Symmetry Breaking. Phys. Rev. Lett., 48:1220–1223, 1982.

[29] D. Kazanas. Dynamics of the Universe and Spontaneous Symmetry Breaking. ApJ, 241:L59–L63, 1980.

[30] A. A. Starobinsky. A New Type of Isotropic Cosmological Models Without Singularity. *Phys.Lett.B*, 91:99–102, 1980.

[31] K. Sato. Cosmological Baryon Number Domain Structure and the First Order Phase Transition of a Vacuum. *Phys.Lett.B*, 99:66–70, 1981.

[32] K. Sato. First Order Phase Transition of a Vacuum and Expansion of the Universe. MNRAS, 195:467–479, 1981.

[33] Viatcheslav F. Mukhanov and G. V. Chibisov. Quantum Fluctuation and Nonsingular Universe. (In Russian). *JETP Lett.*, 33:532–535, 1981.

[34] Viatcheslav F. Mukhanov. CMB, quantum fluctuations and the predictive power of inflation. 2003.

[35] Andrei D. Linde. Chaotic Inflation. *Phys.Lett.B*, 129:177–181, 1983.

[36] E. W. Kolb and M. S. Turner. *The Early Universe*, 1990. Addison-Wesley, Frontiers in Physics, 69.

[37] T. W. B. Kibble. Topology of cosmic domains and strings. Journal of Physics A Mathematical General, 9:1387–1398, August 1976.

[38] G. F. Smoot et al. Structure in the COBE differential microwave radiometer first-year maps. ApJ, 396:L1–L5, September 1992.

[39] Planck Collaboration and P. A. R. Ade et al. Planck 2015 results. XVII. Constraints on primordial non-Gaussianity. arxiv:1502.01592, February 2015.

[40] P. A. R. Ade et al. Planck 2015 results. XX. Constraints on inflation. arxiv:1502.02114, 2015.

[41] W. Hu and N. Sugiyama. Toward understanding CMB anisotropies and their implications. Phys. Rev. D, 51:2599–2630, March 1995.

[42] Marc Kamionkowski, Arthur Kosowsky, and Albert Stebbins. Statistics of cosmic microwave background polarization. Phys. Rev. D, 55:7368–7388, 1997.

[43] Matias Zaldarriaga and Uros Seljak. An all sky analysis of polarization in the microwave background. Phys. Rev. D, 55:1830–1840, 1997.

[44] M. Zaldarriaga and U. Seljak. All-sky analysis of polarization in the microwave background. Phys. Rev. D, 55:1830–1840, February 1997.

[45] M. Kamionkowski, A. Kosowsky, and A. Stebbins. Statistics of cosmic microwave background polarization. Phys. Rev. D, 55:7368–7388, June 1997.

[46] C. Howlett et al. CMB power spectrum parameter degeneracies in the era of precision cosmology. J. Cosmology Astropart. Phys., 1204:027, 2012.

[47] M. Zaldarriaga. Polarization of the microwave background in reionized models. Phys. Rev. D, 55:1822–1829, February 1997.

[48] M. Zaldarriaga and U. Seljak. Gravitational lensing effect on cosmic microwave background polarization. Phys. Rev. D, 58(2):023003, July 1998.

[49] P. A. R. Ade et al. and Polarbear Collaboration. Measurement of the Cosmic Microwave Background Polarization Lensing Power Spectrum with the POLARBEAR Experiment. Phys. Rev. Lett., 113(2):021301, July 2014.

[50] D. Hanson et al. Detection of B-mode Polarization in the Cosmic Microwave Background with Data from the South Pole Telescope. arxiv:astro-ph/1307.5830, July 2013

[51] BICEP2 Collaboration, Keck Array Collaboration, and P. A. R. Ade et al. Improved Constraints on Cosmology and Foregrounds from BICEP2 and Keck Array Cosmic Microwave Background Data with Inclusion of 95 GHz Band. Phys. Rev. Lett., 116(3):031302, January 2016.

[52] W. H. Kinney. TASI Lectures on Inflation. arXiv:0902.1529v2, February 2009.

[53] D. Baumann. TASI Lectures on Inflation. arXiv:0907.5424v2, July 2009.

[54] J. Martin and D. J. Schwarz. WKB approximation for inflationary cosmological perturbations. Phys. Rev. D, 67(8):083512, April 2003.

[55] James E. Lidsey, Andrew R. Liddle, Edward W. Kolb, Edmund J. Copeland, Tiago Barreiro, et al. Reconstructing the inflation potential : An overview. *Rev.Mod.Phys.*, 69:373–410, 1997.

[56] Mark B. Hoffman and Michael S. Turner. Kinematic constraints to the key inflationary observables. Phys. Rev. D, 64:023506, 2001.

[57] William H. Kinney. Inflation: Flow, fixed points and observables to arbitrary order in slow roll. Phys. Rev. D, 66:083508, 2002.

[58] Y. B. Zeldovich. A hypothesis, unifying the structure and the entropy of the universe. MNRAS, 160:1–3, 1972.

[59] E. R. Harrison. Fluctuations at the threshold of classical cosmology. Phys. Rev. D, 1:2726–2730, May 1970.

[60] A. R. Liddle and D. H. Lyth. The cold dark matter density perturbation. Phys. Rep., 231:1–105, August 1993.

[61] R. K. Sachs and A. M. Wolfe. Perturbations of a Cosmological Model and Angular Variations of the Microwave Background. ApJ, 147:73, January 1967.

[62] M. Zaldarriaga and U. Seljak. All-sky analysis of polarization in the microwave background. Phys. Rev. D, 55:1830–1840, Feb 1997.

[63] BICEP2 Collaboration, Keck Array Collaboration, and P. A. R. Ade et al. Improved Constraints on Cosmology and Foregrounds from BICEP2 and Keck Array Cosmic Microwave Background Data with Inclusion of 95 GHz Band. Phys. Rev. Lett., 116(3):031302, January 2016.

[64] Steven Weinberg. Damping of tensor modes in cosmology. Phys. Rev. D, 69:023503, 2004.

[65] L. A. Boyle and P. J. Steinhardt. Probing the early universe with inflationary gravitational waves. Phys. Rev. D, 77:063504, Mar 2008.

[66] M. Maggiore. Gravitational wave experiments and early universe cosmology. *Phys. Rep.*, 331(6):283 – 367, 2000.

[67] Takahashi T. Kuroyanagi, S. and S. Yokoyama. Blue-tilted tensor spectrum and thermal history of the Universe. J. Cosmology Astropart. Phys., 2:003, February 2015.

[68] R. Allahverdi et al. Reheating in Inflationary Cosmology: Theory and Applications. *Annual Review of Nuclear and Particle Science*, 60:27–51, November 2010.

[69] Chiba T. Kuroyanagi, S. and N. Sugiyama. Precision calculations of the gravitational wave background spectrum from inflation. Phys. Rev. D, 79(10):103501, May 2009.

[70] Jerod Caligiuri and Arthur Kosowsky. Inflationary Tensor Perturbations After BICEP. Phys. Rev. Lett., 112:191302, 2014.

[71] J. Caligiuri et al. Constraining the history of inflation from microwave background polarimetry and laser interferometry. Phys. Rev. D, 91:103529,May 2015.

[72] BICEP2/Keck and Planck Collaborations, P. A. R. Ade et al. Joint Analysis of BICEP2/Keck Array and Planck Data. Phys. Rev. Lett., 114(10):101301, March 2015.

[73] P.A.R. Ade et al. Detection of B-Mode Polarization at Degree Angular Scales by BICEP2. Phys. Rev. Lett., 112:241101, 2014.

[74] M. S. Turner. Detectability of inflation-produced gravitational waves. Phys. Rev. D, 55:435, January 1997.

[75] Carlo Ungarelli, Pierstefano Corasaniti, R.A. Mercer, and Alberto Vecchio. Gravitational waves, inflation and the cosmic microwave background: Towards testing the slow-roll paradigm. *Class.Quant.Grav.*, 22:S955–S964, 2005.

[76] Asantha Cooray. Primordial gravitational waves and inflation: CMB and direct detection with space-based laser interferometers. *Mod.Phys.Lett.A*, 20:2503–2519, 2005.

[77] Tristan L. Smith, Marc Kamionkowski, and Asantha Cooray. Direct detection of the inflationary gravitational wave background. Phys. Rev. D, 73:023504, 2006.

[78] Tristan L. Smith, Hiranya V. Peiris, and Asantha Cooray. Deciphering inflation with gravitational waves: cosmic microwave background polarization vs. direct detection with laser interferometers. Phys. Rev. D, 73:123503, 2006.

[79] Sirichai Chongchitnan and George Efstathiou. Prospects for direct detection of primordial gravitational waves. Phys. Rev. D, D73:083511, 2006.

[80] Brett C. Friedman, Asantha Cooray, and Alessandro Melchiorri. Wmap-normalized inflationary model predictions and the search for primordial gravitational waves with direct detection experiments. Phys. Rev. D, 74:123509, Dec 2006.

[81] J. E. Lidsey et al. Reconstructing the inflaton potential-an overview. *Rev. Mod. Phys.*, 69:373–410, April 1997.

[82] ACT Collaboration and J. L. Sievers et al. The Atacama Cosmology Telescope: cosmological parameters from three seasons of data. J. Cosmology Astropart. Phys., 10:60, October 2013.

[83] Z. Hou et al. Constraints on Cosmology from the Cosmic Microwave Background Power Spectrum of the 2500 deg^2 SPT-SZ Survey. ApJ, 782:74, February 2014.

[84] Planck Collaboration and P. A. R. Ade et al. Planck 2013 results. XVI. Cosmological parameters. March 2013.

[85] A. R. Liddle and D. Lyth. Cobe, gravitational waves, inflation and extended inflation. *Phys. Lett. B*, 291(4):391 – 398, 1992.

[86] Matias Zaldarriaga and Uro Seljak. Gravitational lensing effect on cosmic microwave background polarization. Phys. Rev. D, 58:023003, Jun 1998.

[87] L. Knox and Y.-S. Song. Limit on the Detectability of the Energy Scale of Inflation. Phys. Rev. Lett., 89(1):011303, July 2002.

[88] W. Hu and T. Okamoto. Mass Reconstruction with Cosmic Microwave Background Polarization. ApJ, 574:566–574, August 2002.

[89] C. M. Hirata and U. Seljak. Reconstruction of lensing from the cosmic microwave background polarization. Phys. Rev. D, 68(8):083002, October 2003.

[90] Y.-S. Song and L. Knox. Detectability of departures from the inflationary consistency equation. Phys. Rev. D, 68(4):043518, August 2003.

[91] L. Verde, H. V. Peiris, and R. Jimenez. Considerations in optimizing CMB polarization experiments to constrain inflationary physics. J. Cosmology Astropart. Phys., 1:19, January 2006.

[92] D. Baumann et al., *American Institute of Physics Conference Series*, Ed. S. Dodelson et al., Vol. 1141, pp. 10-120, 2009.

[93] M. Farhang et al. Primordial Gravitational Wave Detectability with Deep Small-Sky CMB Experiments. arxiv:1108.2043, August 2011.

[94] J. Dunkley et al., *American Institute of Physics Conference Series*, Ed. S. Dodelson et al., Vol. 1141, pp. 222-264. 2009.

[95] BICEP2 Collaboration and P. A. R Ade et al. BICEP2 I: Detection Of B-mode Polarization at Degree Angular Scales. March 2014.

[96] A. Albrecht et al. Report of the Dark Energy Task Force. September 2006.

[97] K. N. Abazajian et al. Neutrino Physics from the Cosmic Microwave Background and Large Scale Structure. *Astroparticle Physics*, 63:66–80, March 2015.

[98] E. S. Phinney et al., "The Big Bang Observer: Direct Detection of Gravitational Waves from the Birth of the Universe to the Present", NASA Mission Concept Study, 2004.

[99] H. Kudoh et al. Detecting a gravitational-wave background with next-generation space interferometers. Phys. Rev. D, 73(6):064006, March 2006.

[100] N. Seto. Correlation analysis of stochastic gravitational wave background around 0.1 1 Hz. Phys. Rev. D, 73(6):063001, March 2006.

[101] Kosowsky A. Kamionkowski, M. and M. Turner. Gravitational radiation from first-order phase transitions. Phys. Rev. D, 49:2837–2851, Mar 1994.

[102] Kahniashvili T. Gogoberidze, G. and A. Kosowsky. Spectrum of gravitational radiation from primordial turbulence. Phys. Rev. D, 76:083002, Oct 2007.

[103] M. Ando et al. *Class. Quant. Grav.*, 27, 2010.

[104] S. Kawamura et al. The Japanese space gravitational wave antenna: DECIGO. Laser interferometer space antenna. Proceedings, 8th International LISA Symposium, Stanford, USA, June 28-July 2, 2010. *Class. Quant. Grav.*, 28:094011, 2011

[105] N. Seto, S. Kawamura, and T. Nakamura. Possibility of Direct Measurement of the Acceleration of the Universe Using 0.1 Hz Band Laser Interferometer Gravitational Wave Antenna in Space. Phys. Rev. Lett., 87(22):221103, November 2001.

[106] A. Kosowsky and M. S. Turner. CBR anisotropy and the running of the scalar spectral index. Phys. Rev. D, 52:1739, August 1995.

[107] Raphael Flauger, J. Colin Hill, and David N. Spergel. Toward an Understanding of Foreground Emission in the BICEP2 Region. J. Cosmology Astropart. Phys., 1408, 2014.

[108] Michael J. Mortonson and Uro Seljak. A joint analysis of Planck and BICEP2 B modes including dust polarization uncertainty. arxiv:1405.5857, 2014.

[109] Planck Collaboration, R. Adam et al. Planck intermediate results. XXX. The angular power spectrum of polarized dust emission at intermediate and high Galactic latitudes. A&A, 586:A133, February 2016.

[110] BICEP2/Keck and Planck Collaborations, P. A. R. Ade et al. Joint Analysis of BICEP2/Keck Array and Planck Data. Phys. Rev. Lett., 114(10):101301, March 2015.

[111] Michael S. Turner. Detectability of inflation produced gravitational waves. Phys. Rev. D, 55:435–439, 1997.

[112] Sachiko Kuroyanagi, Shinji Tsujikawa, Takeshi Chiba, and Naoshi Sugiyama. Implications of the B-mode Polarization Measurement for Direct Detection of Inflationary Gravitational Waves. Phys. Rev. D, 90:063513, September 2014.

[113] Ryusuke Jinno, Takeo Moroi, and Tomo Takahashi. Studying Inflation with Future Space-Based Gravitational Wave Detectors. arxiv:1406.1666, December 2014.

[114] L. Boyle et al. Testing and extending the inflationary consistency relation for tensor modes. Phys. Rev. D, 92:043504, August 2015.

[115] R. Easther and W. H. Kinney. Monte carlo reconstruction of the inflationary potential. Phys. Rev. D, 67:043511, 2003.

[116] Carlo R. Contaldi. BICEP's acceleration. *JCAP*, 1410(10):072, 2014.

[117] P.A.R. Ade et al. Planck 2013 results. XVI. Cosmological parameters. *å*, 571:A16, 2014.

[118] Ewan D. Stewart and David H. Lyth. A More accurate analytic calculation of the spectrum of cosmological perturbations produced during inflation. *Phys.Lett.B*, 302:171–175, 1993.

[119] D.N. Spergel et al. First year Wilkinson Microwave Anisotropy Probe (WMAP) observations: Determination of cosmological parameters. ApJS, 148:175–194, 2003.

[120] C.L. Bennett et al. Nine-Year Wilkinson Microwave Anisotropy Probe (WMAP) Observations: Final Maps and Results. ApJS, 208:20, 2013.

[121] Christopher P. Ahn et al. The Ninth Data Release of the Sloan Digital Sky Survey: First Spectroscopic Data from the SDSS-III Baryon Oscillation Spectroscopic Survey. ApJS, 203:21, 2012.

[122] D. H. Jones et al. The 6dF Galaxy Survey: Final Redshift Release (DR3) and Southern Large-Scale Structures. MNRAS, 399:683–698, October 2009.

[123] Chris Blake, Eyal Kazin, Florian Beutler, Tamara Davis, David Parkinson, et al. The WiggleZ Dark Energy Survey: mapping the distance-redshift relation with baryon acoustic oscillations. MNRAS, 418:1707–1724, 2011.

[124] K. Freese and W. H. Kinney. Natural Inflation: Consistency with Cosmic Microwave Background Observations of Planck and BICEP2. J. Cosmology Astropart. Phys., 3:044, March 2015.

[125] Tristan L. Smith, Marc Kamionkowski, and Asantha Cooray. The inflationary gravitational-wave background and measurements of the scalar spectral index. Phys. Rev. D, 78:083525, 2008.

[126] Yuki Watanabe and Eiichiro Komatsu. Improved Calculation of the Primordial Gravitational Wave Spectrum in the Standard Model. Phys. Rev. D, 73:123515, 2006.

[127] S. Kawamura, T. Nakamura, M. Ando, N. Seto, K. Tsubono, et al. The Japanese space gravitational wave antenna DECIGO. *Class.Quant.Grav.*, 23:S125–S132, 2006.

[128] Lloyd Knox and Yong-Seon Song. A Limit on the detectability of the energy scale of inflation. Phys. Rev. Lett., 89:011303, 2002.

[129] Christopher M. Hirata and Uros Seljak. Reconstruction of lensing from the cosmic microwave background polarization. Phys. Rev. D, 68:083002, 2003.

[130] A. Kogut et al. The Primordial Inflation Explorer (PIXIE): a nulling polarimeter for cosmic microwave background observations. J. Cosmology Astropart. Phys., 7:25, July 2011.

[131] Sachiko Kuroyanagi, Takeshi Chiba, and Naoshi Sugiyama. Prospects for Direct Detection of Inflationary Gravitational Waves by Next Generation Interferometric Detectors. Phys. Rev. D, 83:043514, 2011.

[132] Liang Dai, Marc Kamionkowski, and Junpu Wang. Reheating constraints to inflationary models. Phys. Rev. Lett., 113:041302, 2014.

[133] Planck Collaboration and P. A. R. Ade et al. Planck intermediate results. XXXVIII. E- and B-modes of dust polarization from the magnetized filamentary structure of the interstellar medium. *å*, 586:A141, February 2016.

[134] Dickinson C. Remazeilles, M., H. K. K. Eriksen, and I. K. Wehus. Sensitivity and foreground modelling for large-scale cosmic microwave background B-mode polarization satellite missions. MNRAS, 458:2032–2050, May 2016.

[135] M. D. Niemack et al. BFORE: The B-mode Foreground Experiment. *Journal of Low Temperature Physics*, December 2015.

[136] C. The COrE Collaboration, Armitage-Caplan et al. COrE (Cosmic Origins Explorer) A White Paper. arxiv:1102.2181, February 2011.

[137] T. Matsumura et al. Mission Design of LiteBIRD. *Journal of Low Temperature Physics*, 176:733–740, September 2014.

[138] J. Bock et al. Study of the Experimental Probe of Inflationary Cosmology (EPIC)-Intemediate Mission for NASA's Einstein Inflation Probe. arxiv:0906.1188, June 2009.

[139] PRISM Collaboration and P. Andre et al. PRISM (Polarized Radiation Imaging and Spectroscopy Mission): A White Paper on the Ultimate Polarimetric Spectro-Imaging of the Microwave and Far-Infrared Sky. arxiv:1306.2259, June 2013.

[140] M. Zaldarriaga and U. Seljak. Gravitational lensing effect on cosmic microwave background polarization. Phys. Rev. D, 58(2):023003, July 1998.

[141] A. van Engelen et al. A Measurement of Gravitational Lensing of the Microwave Background Using South Pole Telescope Data. ApJ, 756:142, September 2012

[142] M. Madhavacheril et al. and the Atacama Cosmology Telescope Collaboration. Evidence of Lensing of the Cosmic Microwave Background by Dark Matter Halos. Phys. Rev. Lett., 114:151302, April 2015.

[143] A. van Engelen et al. and the Atacama Cosmology Telescope Collaboration. The Atacama Cosmology Telescope: Lensing of CMB Temperature and Polarization Derived from Cosmic Infrared Background Cross-correlation. ApJ, 808:7, July 2015.

[144] R. E. Smith et al. Stable clustering, the halo model and non-linear cosmological power spectra. MNRAS,341:1311–1332, June 2003

[145] F. Bernardeau, L. van Waerbeke, and Y. Mellier. Weak lensing statistics as a probe of {OMEGA} and power spectrum. A&A, 322:1–18,June 1997.

[146] A. Amara et al. The COSMOS density field: a reconstruction using both weak lensing and galaxy distributions. MNRAS, 424:553–536, July 2012.

[147] C. Chang et al.. Galaxy bias from the Dark Energy Survey Science Verification data: combining galaxy density maps and weak lensing maps. MNRAS, 459:3203–3216, July 2016.

[148] T. Keck Array and P. A. R. BICEP2 Collaborations, Ade et al. BICEP2 / Keck Array VIII: Measurement of gravitational lensing from large-scale B-mode polarization. arxiv:1606.01968, June 2016.

[149] B. P. collaboration = LIGO Scientific Collaboration and Virgo Collaboration, Abbott et al. Observation of gravitational waves from a binary black hole merger. Phys. Rev. Lett., 116:6, February 2016.

[150] B. Helou et al. LISA pathfinder appreciably constrains collapse models. arxiv:1606.03637, June 2016.

[151] P. Amaro-Seoane et al. eLISA: Astrophysics and cosmology in the millihertz regime. *GW Notes*, 6:4–110, May 2013.

[152] T. Regimbau. The astrophysical gravitational wave stochastic background. *Research in Astronomy and Astrophysics*, 11:369–390, April 2011.

[153] M. H. Gregory et al. Laser interferometry for the big bang observer. *Class. Quant. Grav.*, 23(15):4887, 2006.

[154] X.-J. Liu et al. Detecting relic gravitational waves by pulsar timing arrays: Effects of cosmic phase transitions and relativistic free-streaming gases. Phys. Rev. D, 93(2):024031, January 2016.

[155] W. Zhao et al. Constraints of relic gravitational waves by pulsar timing arrays: Forecasts for the FAST and SKA projects. Phys. Rev. D, 87(12):124012, June 2013.

[156] A. P. Hearin, A. R. Zentner and Z. Ma. General requirements on matter power spectrum predictions for cosmology with weak lensing tomography. J. Cosmology Astropart. Phys., 4:034, April 2012.

[157] R Laureijs et al. Euclid Definition Study Report. arxiv:1110.3193, October 2011.

[158] LSST Science Collaboration and P. A. Abell et al. LSST Science Book, Version 2.0. arxiv:0912.0201, December 2009.

[159] S. More. How Accurate is Our Knowledge of the Galaxy Bias? ApJ, 741:19, November 2011.

[160] S. More et al. The galaxy-dark matter connection: A cosmological perspective. *Journal of Physics Conference Series*, 484(1):012042, March 2014.

[161] F. Bernardeau et al. Large-scale structure of the Universe and cosmological perturbation theory. Phys. Rep., 367:1–248, September 2002.

[162] J. C. Pober et al. What Next-generation 21 cm Power Spectrum Measurements can Teach us About the Epoch of Reionization. ApJ, 782:66, February 2014.

[163] K. Kohri et al. Precise measurements of primordial power spectrum with 21 cm fluctuations. J. Cosmology Astropart. Phys., 10:065, October 2013.

[164] A. Liu and A. R. Parsons. Constraining cosmology and ionization history with combined 21 cm power spectrum and global signal measurements. MNRAS, 457:1864–1877, April 2016.

[165] M. Tegmark and M. Zaldarriaga. Omniscopes: Large area telescope arrays with only N$\log N$ computational cost. Phys. Rev. D, 82(10):103501, November 2010.

[166] A. Borde et al. New approach for precise computation of Lyman-α forest power spectrum with hydrodynamical simulations. J. Cosmology Astropart. Phys., 7:005, July 2014.

[167] N. Palanque-Delabrouille et al. Neutrino masses and cosmology with Lyman-alpha forest power spectrum. J. Cosmology Astropart. Phys., 11:011, November 2015.

[168] S. Zaroubi et al. The matter power spectrum from the Lyα forest: an optical depth estimate. MNRAS, 369:734–750, June 2006.

[169] Erickcek A. L. Li, F. and N. M. Law. A new probe of the small-scale primordial power spectrum: astrometric microlensing by ultracompact minihalos. Phys. Rev. D, 86:043519, 2012.

[170] Y. Yang. Constraints on the primordial power spectrum of small scales using the neutrino signals from the dark matter decay. arxiv:1501.00789, January 2015.

[171] A. Natarajan, N. Zhu and N. Yoshida. Probing the Small Scale Matter Power Spectrum through Dark Matter Annihilation in the Early Universe. arxiv:1503.03480, March 2015.

[172] R. Feldmann and D. Spolyar. Detecting dark matter substructures around the Milky Way with Gaia. MNRAS, 446:1000–1012, January 2015.

[173] Knebe A. Warnick, K. and C. Power. The tidal streams of disrupting subhaloes in cosmological dark matter haloes. MNRAS, 385:1859–1883, April 2008.

[174] D. Erkal and V. Belokurov. Properties of dark subhaloes from gaps in tidal streams. MNRAS, 454:3542–3558, December 2015.

[175] J. Chluba, A. L. Erickcek and I. Ben-Dayan. Probing the Inflaton: Small-scale Power Spectrum Constraints from Measurements of the Cosmic Microwave Background Energy Spectrum. ApJ, 758:76, October 2012

[176] R. Khatri and R. A. Sunyaev. Forecasts for CMB μ and i-type spectral distortion constraints on the primordial power spectrum on scales 8lesssimklesssim10^4 Mpc^{-1} with the future Pixie-like experiments. J. Cosmology Astropart. Phys., 6:026, June 2013